http://www.kidney-international.org

A role of liver fatty acid-binding protein in cisplatin-induced acute renal failure

K Negishi[1], E Noiri[1], T Sugaya[2], S Li[3], J Megyesi[3], K Nagothu[3] and D Portilla[3]

[1]Department of Nephrology and Endocrinology, University of Tokyo, Tokyo, Japan; [2]CMIC Ltd, Tokyo, Japan and [3]Division of Nephrology, Department of Internal Medicine, University of Arkansas for Medical Sciences and Central Arkansas Veterans Healthcare System, Little Rock, Arkansas, USA

Previous studies from our laboratory showed that increased fatty acid oxidation by the kidney is cytoprotective during cisplatin (CP)-mediated nephrotoxicity. In this study, we determined the effects of CP and fibrates on peroxisome proliferation and the expression of liver fatty acid-binding protein (L-FABP) in normal mice, and in mice transgenically overexpressing human L-FABP (h-L-FABP). Labeling of peroxisomes demonstrated reduced peroxisomal staining in the proximal tubule of CP-treated mice compared with control mice. There was increased peroxisomal labeling in the proximal tubules of both control and CP-treated mice when either was treated with fibrate; a known peroxisome proliferator-activated receptor-α ligand. L-FABP protein expression, not detected in control or CP-treated mice, was significantly increased in the proximal tubules of fibrate-treated mice of either group. In the transgenic mice, CP increased the shedding of h-L-FABP in the urine, which was decreased by fibrate as was the acute renal failure.
A cytosolic pattern of h-L-FABP expression was found in the proximal tubules of untreated transgenic mice with a nuclear presence in CP-treated mice. Fibrate pretreatment restored the cytosolic expression pattern in CP-treated mice. Our study shows that fibrate may improve CP-induced acute renal failure due to both peroxisome proliferation and increased L-FABP in the cytosol of the proximal tubule.

Kidney International (2007) **72,** 348–358; doi:10.1038/sj.ki.5002304; published online 9 May 2007

KEYWORDS: acute renal failure; cisplatin nephrotoxicity; lipids

Correspondence: *D Portilla, Department of Medicine, University of Arkansas for Medical Sciences, Slot 501, 4301 W. Markham St, Little Rock, Arkansas 72205, USA. E-mail: portilladidier@uams.edu*

Received 17 January 2007; revised 9 March 2007; accepted 20 March 2007; published online 9 May 2007

The intracellular fatty acid-binding proteins (FABPs) belong to a super family of lipid-binding proteins with low molecular weight (14–15 kDa), which are classified according to their predominant tissue localization. There are nine different FABPs, with tissue-specific distribution that include L (liver), I (intestinal), H (muscle and heart), A (adipocyte), E (epidermal), Il (ileal), B (brain), M (myelin), and T (testis).[1] The liver isoform of FABP (L-FABP) is highly expressed in hepatocytes, where it represents 5% of the total cytosolic protein. L-FABP facilitates the cellular uptake, transport, and metabolism of fatty acids, and is also involved in the regulation of gene expression and cell differentiation.[2–5] Previous work in liver tissue has shown (1) that the level of L-FABP expression in rodent liver is regulated in concert with peroxisome proliferation and (2) that the transcription rate of L-FABP gene is regulated and induced by both fibrate hypolipidemic drugs and long-chain fatty acids, through a peroxisome proliferator-activated receptor (PPAR)-responsive element located in its promoter region.[6,7]

Although the kidney in rodents does not synthesize a significant amount of L-FABP protein,[8] recent work suggests that L-FABP under normal conditions resides in the lysosomal compartment of the proximal tubule, but also can be reabsorbed from the glomerular filtrate via megalin, a multiligand proximal tubule endocytic receptor.[9] On the other hand, the amount of L-FABP protein present in human kidney is considerably much higher than the amount of L-FABP protein present in rodent kidney tissue, and its expression is restricted to the proximal convoluted and straight tubules.[10,11] In more recent studies using human L-FABP (h-L-FABP) transgenic mice, which express higher protein levels of h-L-FABP in proximal tubules when compared with non-transgenic mice, Noiri *et al.*[12,13] demonstrated that the shedding of h-L-FABP was increased in urine obtained from mice that underwent ischemia–reperfusion injury. Immunohistochemical analysis of kidney tissue of h-L-FABP transgenic mice subjected to ischemia–reperfusion injury demonstrated increased translocation of h-L-FABP from the cytoplasm of the proximal tubule to the tubular lumen. In addition, renal function and histological scores of acute kidney injury, in h-L-FABP transgenic mice subjected to ischemia–reperfusion injury, were significantly ameliorated

when compared with wild-type mice. The role of L-FABP in acute kidney injury caused by cisplatin (CP) has not been examined previously.

In previous studies, we have documented that the inhibition of peroxisomal and mitochondrial fatty acid oxidation (FAO) observed in kidney tissue of mice undergoing ischemia–reperfusion injury and CP-induced acute renal failure (ARF) results from reduced activity of PPARα.[14–20] Failure to oxidize long-chain fatty acids and long-chain acylcarnitines during ARF results in their accumulation and cellular toxicity, which further contributes to proximal tubule cell death.[21,22] In a recent metabolomic study,[23] we found that CP-mediated nephrotoxicity was accompanied by increased serum levels of nonesterified fatty acids and triglycerides, as well as increased accumulation of nonesterified fatty acids and triglycerides in kidney tissue. We also observed that the administration of fibrate, a known PPARα ligand, before ARF (1) prevented the inhibition of FAO and the accumulation of nonesterified fatty acids and triglycerides in kidney tissue, and (2) ameliorated apoptotic and necrotic proximal tubule cell death, which resulted in significant protection of renal function only in PPARα wild-type mice, and not in PPARα null mice.[17–20] Altogether, these previous observations from our laboratory suggest that increased FAO, via PPARα activation, plays a significant role in the observed cytoprotection by fibrates in CP-mediated nephrotoxicity. The cellular targets by which increased PPARα activity in kidney tissue prevents ARF after CP exposure are not currently known.

In these studies, we investigated the contribution of peroxisome proliferation and L-FABP protein expression to the cytoprotective effect of fibrates in the CP model of ARF. For these studies, we used sv-129 mice as well as h-L-FABP transgenic mice. We examined the effects of CP + fibrate on L-FABP expression in kidney tissue and on the shedding of urinary h-L-FABP. In addition, we performed immunohistochemical studies to examine the effects of CP + fibrate on peroxisome proliferation, and the intracellular localization of L-FABP in kidney tissue, and correlated with effects on renal function.

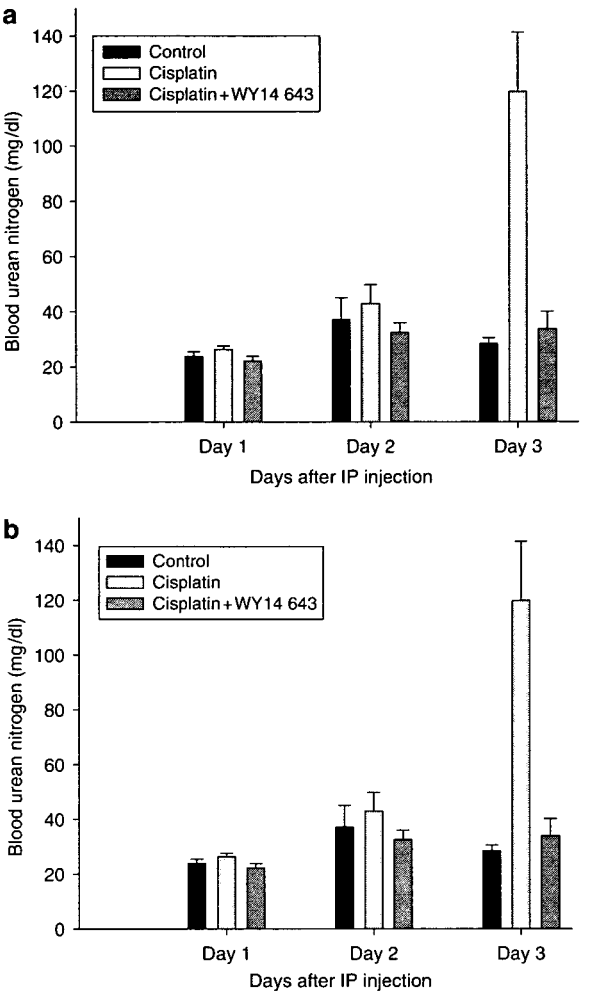

Figure 1 | Effect of fibrate WY-14643 (WY) on renal function in mice after single dose of CP. Mice were fed with either a regular diet or a diet containing 0.1% WY for 7 days before CP administration, as described in Materials and Methods. BUN and creatinine levels were measured at days 1, 2, and 3 after saline (control)-, CP-, or CP + WY-treated mice. Bars correspond to mean ± s.e. of at least six independent experiments under each condition. Changes in (**a**) BUN and (**b**) creatinine levels, respectively, after saline or CP administration in PPARα wild-type mice. *$P<0.005$ when animals were compared with control by unpaired Student's *t*-test.

RESULTS

Studies in sv129 mice

Protective effects of PPARα ligand on CP-induced ARF. Kidney function was monitored by measuring blood urea nitrogen (BUN) and serum creatinine for 3 days after intraperitoneal injection of saline (groups: control and WY) or CP (groups: CP and CP + WY). Figure 1a and b present the changes on BUN and creatinine in mice treated with saline (control), CP, and with WY in the presence of CP. Mice treated with a regular diet and CP developed ARF at day 3 (BUN increased from 28 to 135 and creatinine increased from 0.2 to 1.2 mg/dl). The group of mice that received the WY diet and CP did not develop significant ARF when compared with mice treated with CP alone (BUN increased from 24 on day 1 to 32 and creatinine was unchanged at 0.2 mg/dl after 3 days of CP administration). By contrast, the protective effect of the ligand was lost in PPARα null mice treated with CP (data not shown). PPARα null mice pretreated with a fibrate diet before CP administration developed ARF at day 3. BUN increased from 30 at day 1 to 186 at day 3 and creatinine increased from 0.3 at day 1 to 1.5 mg/dl at day 3.

Effects of CP + fibrates on the expression of 70-kDa peroxisomal membrane protein and peroxisomal matrix protein catalase. We examined by Western blot analysis whether CP or fibrate (WY) treatment had an effect on protein levels of 70-kDa peroxisomal membrane protein (PMP70) or catalase. As shown in Figure 2a, CP-treated mice exhibited a time-dependent reduction in PMP70 protein levels. PMP70

protein levels were reduced by 50% at day 2 and by 75% at day 3 after CP injection. As our studies have shown that the use of PPARα ligand-like fibrates prevent the development of CP-induced proximal tubule cell death by preventing the inhibition of FAO,[14,17] we next examined the effect of fibrate on PMP70 protein levels. As shown in Figure 2b, at day 3 after CP injection, there was a 75% reduction in PMP70 protein levels. In contrast, the group of mice that received the diet containing the fibrate + CP exhibited increased levels of PMP70 by 1.5-fold for fibrate alone, and 1.5-fold for fibrate + CP-treated mice when compared with control untreated mice. We also measured by Western blot analysis protein levels of catalase, a peroxisomal matrix protein. CP at day 3 caused a 30% reduction in expression of a 60-kDa protein corresponding to catalase, and fibrate + CP significantly increased catalase protein expression to levels similar to the ones observed in control untreated mice, as shown in Figure 3.

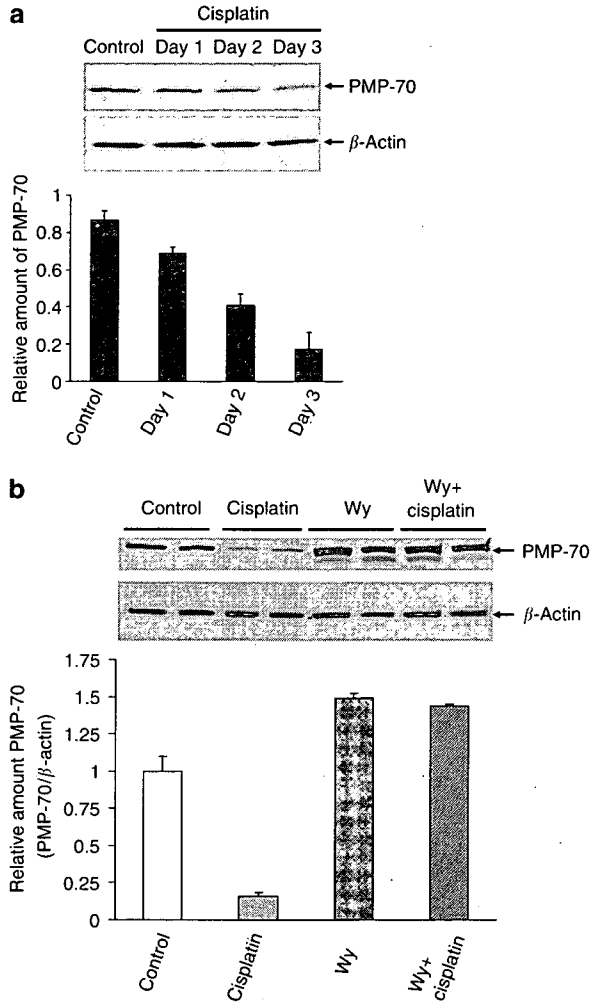

Figure 2 | Effect of fibrate and cisplatin on PMP70 expression in kidney tissue. (**a**) Time course of the effect of CP on PMP70 protein expression in kidney tissue. Mice were administered saline (control) or CP (20 mg/kg body weight) by a single intraperitoneal injection. Western blot analysis of kidney tissue homogenates at days 1, 2, and 3 after CP injection using a PMP70 antibody as described in Materials and Methods. Bars correspond to mean ± s.e. of at least three independent experiments under each condition. (**b**) Effect of fibrate (WY) and CP on PMP70 protein expression. Mouse kidney tissue homogenates were prepared from animals subjected to four experimental conditions, and Western blots were performed as described in Materials and Methods. PMP-70 protein levels were normalized using β-actin as internal control. Bars correspond to mean ± s.e. of at least three independent experiments under each condition.

Image analysis of quantum dot peroxisome fluorescence from kidneys of fibrate-treated mice. To determine the effects of CP + fibrate on peroxisome proliferation, we used a recently developed method for immunofluorescent staining of peroxisomes and quantification of peroxisome fluorescence using an antibody to the PMP70 coupled with fluorescent nanocrystals, Quantum Dots™.[24] The quantum dot peroxisome fluorescence information is contained in the red channel of the RGB image, so quantification is performed in the red channel using a confocal microscope. As shown in Figure 4a, the pixel intensity of red/orange quantum dots was predominantly observed in the proximal tubules of control untreated mice ($15 \times 10^3 \pm 1406$ pixel fluorescent units) and was significantly elevated in fibrate (WY)-treated mice ($21 \times 10^3 \pm 1256$ pixel fluorescent units; Figure 4b). The intensity of pixels was significantly reduced in CP-treated animals ($1.7 \times 10^3 \pm 803$ pixel fluorescent units; Figure 4c) when compared with fibrate (WY) + CP-treated mice $19 \times 10^3 \pm 1167$ pixel fluorescent units; Figure 4d). Figure 4e summarizes data obtained from four separate experiments.

Effect of CP on mouse L-FABP mRNA levels in kidney tissue of sv129 mice. We next examined the effects of CP on mRNA expression of mouse L-FABP (mL-FABP) in kidney tissue of sv129 mice. As shown in Figure 5, by real-time reverse transcriptase-polymerase chain reaction quantitative analysis, after 3 days of CP injection, there was a mild (1.5–1.8-fold)

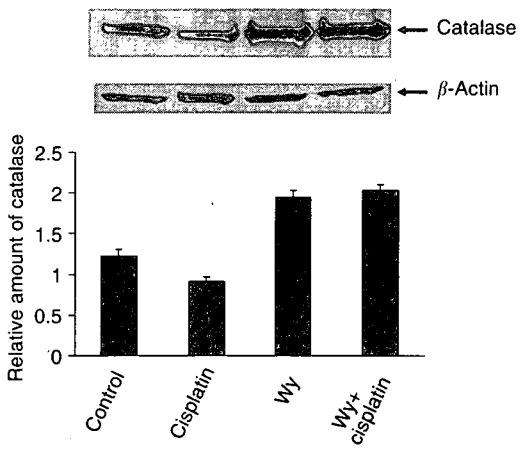

Figure 3 | Effect of fibrate (WY) and CP on catalase protein expression. Mouse kidney tissue homogenates were prepared from animals subjected to four experimental conditions, and Western blots were performed as described in Materials and Methods. Catalase protein levels were normalized using β-actin as internal control. Bars correspond to mean ± s.e. of at least three independent experiments under each condition.

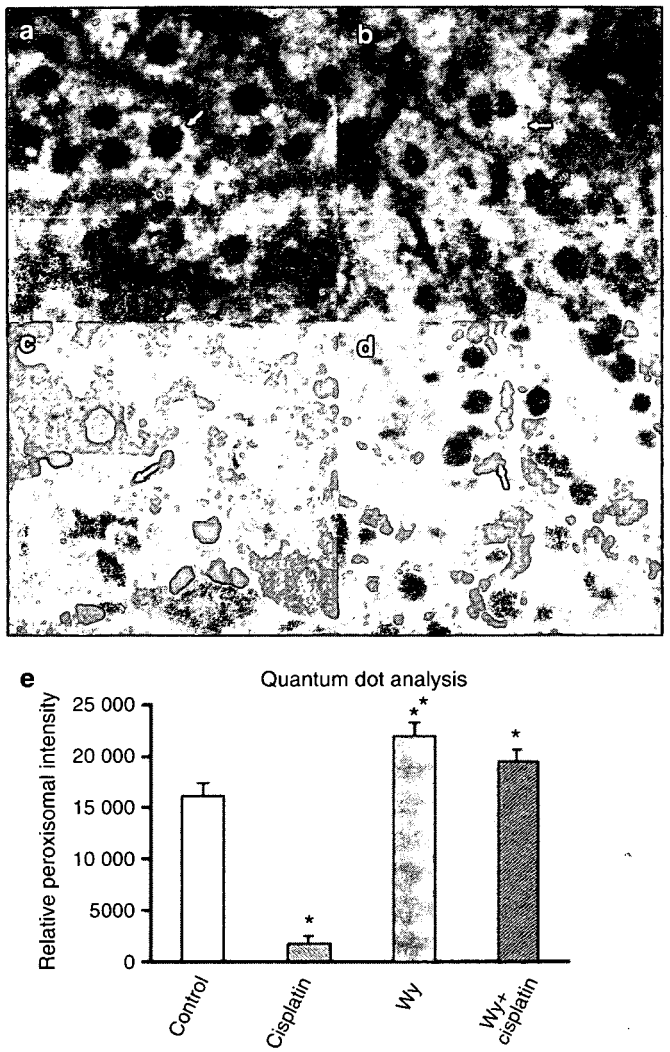

Figure 4 | Effect of fibrate (WY) and CP on peroxisomal distribution. (**a**) Mouse kidney sections from animals subjected to four experimental conditions (**a**) control, (**b**) fibrate (WY), (**c**) CP, and (**d**) WY + CP were stained with PMP70 antibody as described in Materials and Methods. (**e**) Quantitative analysis of pixel densities of the peroxisomal population present in the four experimental conditions was performed as described in the Materials and Methods section. Bars correspond to mean ± s.e. of at least four independent experiments under each condition.

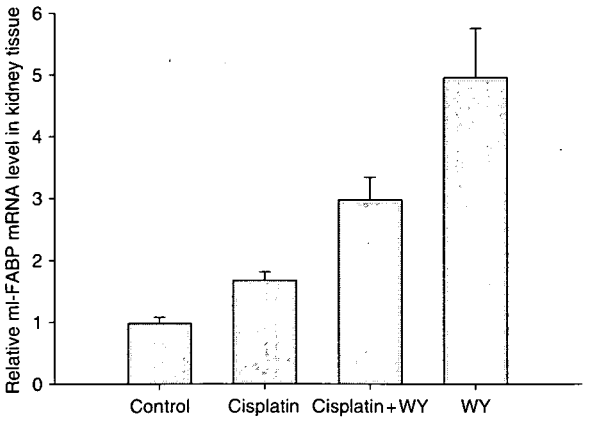

Figure 5 | Effect of CP and fibrate on mL-FABP mRNA levels in SV-129 wild-type mice. Mice that received either a normal diet or a diet containing fibrate (WY) for 7 days were injected with saline (control) or CP and then killed at the indicated times. Levels of mL-FABP mRNA was measured by real-time reverse transcriptase-polymerase chain reaction as described in Materials and Methods. Figure shows relative mL-FABP gene expression in saline (control), CP-, CP + fibrate-, and fibrate-treated mice normalized by 28S rRNA expression. Values are mean ± s.e. mRNA levels. Data were obtained from at least three independent experiments.

increase in the mL-FABP mRNA levels when compared with saline-treated mice. In kidney tissue of sv129 mice treated with CP + fibrate, there was a 3.0-fold increase on L-FABP mRNA levels ($P<0.01$), and fibrate alone upregulated L-FABP mRNA expression by fivefold ($P<0.01$) when compared with saline-treated mice.

Fibrate increases L-FABP protein expression in kidney tissue of PPARα wild type but not on PPARα null mice. Using antibodies that recognize mL-FABP and kidney tissue isolated from sv129 mice treated with CP + fibrate (WY), we found that protein expression of mL-FABP, which was not detected in kidney tissue of untreated or CP-treated sv129 mice, was significantly induced in the proximal tubules of PPARα wild-type mice treated with the fibrate, in the absence and presence of CP. Western blot analysis of mL-FABP, shown in Figure 6a, demonstrates that L-FABP protein was not detected in control or CP-treated sv129 mice. However, treatment of sv129 mice with PPARα ligand WY led to a rapid increase in the expression of mL-FABP. Even though CP treatment slightly reduced expression of L-FABP protein level, it remained significantly elevated in the presence of PPARα ligand WY. By contrast, mL-FABP expression was not detected in kidney tissue of PPARα null mice treated with fibrates, where we did not see protection from CP-induced ARF, as shown in Figure 6b.

Immunohistochemical localization of mL-FABP. Immunohistology of normal mouse kidney cortex demonstrated no positive L-FABP staining (Figure 7a). As shown in Figure 7b, L-FABP is highly expressed in Bowman capsule and early proximal tubule cells of WY-treated animals. In fibrate-treated sv129 mice, a strongly positive staining was seen in the cytosol and perinuclear localization. Only occasional, single cell-positive staining could be seen in CP-treated animals in intact proximal tubules (Figure 7c). Similarly to the WY-treated animals, the positive L-FABP immunoreactivity was detected in Bowman capsule and early proximal tubule cells in kidneys from WY + CP-treated mice (Figure 7d). There was no positive staining in glomeruli and distal nephron segments.

Studies in h-L-FABP transgenic mice

Effects of CP + fibrate on renal function in h-L-FABP transgenic mice. To further examine the regulation of L-FABP expression in mouse kidney tissue, we used h-L-FABP transgenic mice. These mice express higher levels of h-L-FABP protein

in the cytosolic compartment of the proximal tubule when compared with non-transgenic mice, and do not exhibit a particular histologic or functional renal phenotype. In previous published studies using these same h-L-FABP transgenic mice, Noiri[13] and Kamijo *et al.*[25] demonstrate that acute kidney injury due to ischemia–reperfusion injury and unilateral ureteral obstruction was significantly ameliorated when compared with wild-type non-transgenic mice. CP was administered at a dose of 20 mg/kg body weight, and fibrate was administered as a diet containing 0.5% bezafibrate (Bz) for 7 days before the administration of CP. Figure 8a and b present the changes on BUN and creatinine in h-L-FABP transgenic mice treated with saline (control), CP, and with Bz in the absence and presence of CP. Mice treated with a regular diet and CP developed ARF at day 3 (BUN increased from 24 to 143 and creatinine increased from 0.15 to 1.50 mg/dl). The group of mice that received the Bz diet and CP were significantly protected from CP nephrotoxicity, when compared with mice treated with CP alone (BUN increased from 24 to 62 and creatinine increased from 0.15 to 0.47 mg/dl).

Effect of CP + fibrate on shedding of urinary h-L-FABP. In h-L-FABP transgenic mice treated with CP, analysis of urinary h-L-FABP protein by enzyme-linked immunosorbent assay demonstrated a time-dependent increase in the shedding of urinary h-L-FABP protein, which was detected within the first 24 h after CP administration ($n = 12$). Figure 9 shows the time course of shedding of urinary h-L-FABP after CP or

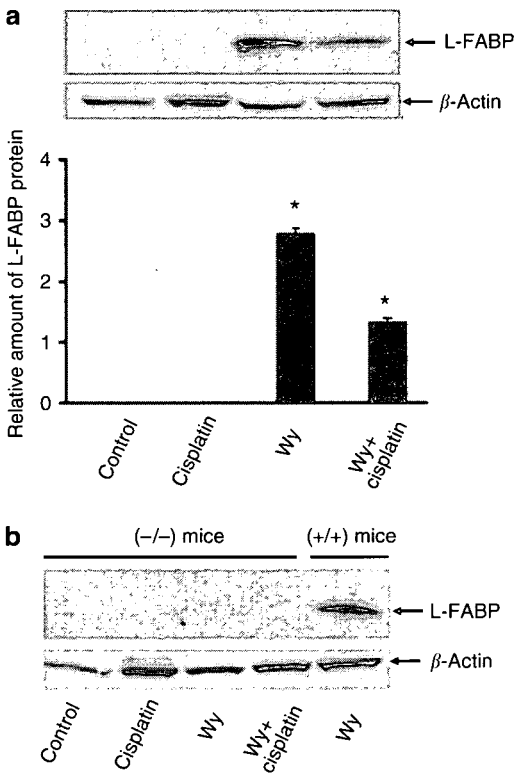

Figure 6 | Effect of CP and Wy on L-FABP protein levels in SV-129 wild-type (+/+) and PPARα null (−/−) mice. (**a**) Effect f of CP and WY on L-FABP protein levels in SV-129 wild-type (+/+) mice. The immunoblot analysis of mouse kidney tissue homogenates from four different experimental conditions was performed as described in Materials and Methods. β-Actin antibody was used as an internal control for normalizing the L-FABP protein levels. Bars correspond to mean ± s.e. of at least three independent experiments under each condition. *$P < 0.005$ when animals were compared with control by unpaired Student's *t*-test. (**b**) Effect f of CP and fibrate on L-FABP protein levels in sv-129 PPARα knock out (−/−) mice. The immunoblot analysis of mouse kidney tissue homogenates from four different experimental conditions was performed as described in Materials and Methods. Kidney homogenate from wild-type mice treated with fibrate (WY) was run as positive control for L-FABP protein. β-Actin antibody was used as an internal control for normalizing the L-FABP protein levels.

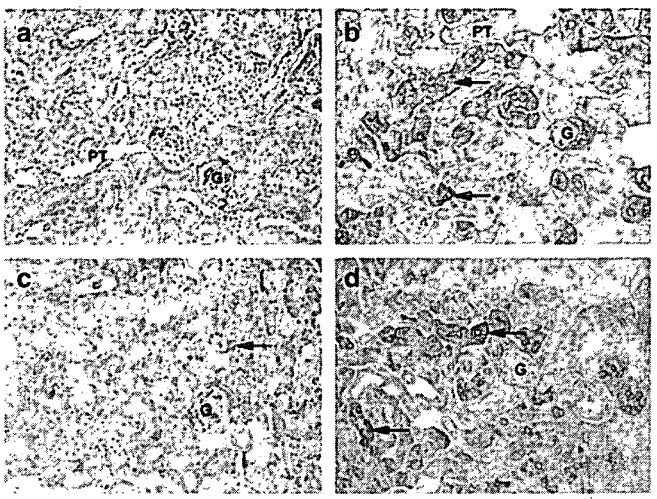

Figure 7 | Immunolocalization of mL-FABP. Representative picture of kidney sections from (**a**) control-, (**b**) fibrate (WY)-, (**c**) CP-, and (**d**) WY + CP-treated mice stained with anti-mL-FABP antibody. Positive immunostaining was apparent only in fibrate and fibrate + CP-treated mice predominantly in proximal tubules (PT) of the outer cortex (arrows). Original magnification × 122.

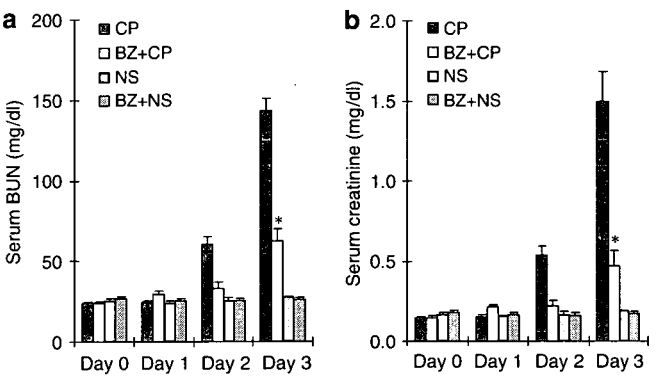

Figure 8 | Effect of Bz on renal function in h-L-FABP transgenic mice after single dose of CP. Mice were fed with either a regular diet or a diet containing 0.1% Bz for 7 days before CP administration, as described in Materials and Methods. BUN and creatinine levels were measured at days 1, 2, and 3 after saline control (NS)-, CP (CP)-, CP + Bz (CP + BZ)-, or saline + Bz (BZ + NS)-treated mice. Bars correspond to means ± s.e. of at least 10 independent experiments under each condition. (**a**) Changes in BUN and (**b**) creatinine levels, respectively, after saline or CP administration in PPARα wild-type mice. *$P < 0.05$ when CP + Bz group was compared with CP alone group by unpaired Student's *t*-test.

saline administration. In CP-treated h-L-FABP transgenic mice, urinary h-L-FABP levels increased by 100-fold at day 1 after CP injection, from baseline levels of 13.6 $\mu g/g$ creatinine in saline-treated mice to 1334.9 $\mu g/g$ creatinine in CP-treated mice. At 3 days after CP injection, urinary h-L-FABP levels did increase by 647-fold from baseline level of 12.9–8422 $\mu g/g$ creatinine. Urinary levels of h-L-FABP were significantly reduced in the Bz + CP-treated group when compared with CP-treated mice (urinary h-L-FABP levels were reduced from 8422 to 1120 $\mu g/g$ creatinine at day 3 after CP administration). Statistical significance between different time points in the same group was evaluated by paired *t*-test, and the statistical significance between two separate groups was evaluated by analysis of variance. Our results suggest that the increased shedding of h-L-FABP protein in urine samples obtained from CP-treated h-L-FABP transgenic mice precedes changes in serum creatinine or BUN, which were not detected until 2–3 days after CP administration as shown in Figure 8. Our results also show that very small amounts of urinary h-L-FABP are also shed by the administration of a PPARα ligand.

Immunohistochemical localization of h-L-FABP in h-L-FABP transgenic mice. There was no positive immunoreactivity for h-L-FABP in kidneys from control C57Bl wild-type non-transgenic mice (Figure 10a). Untreated h-L-FABP transgenic animals showed strong positive staining in the cytoplasm of early (S1 and S2) segments of proximal tubules, with occasional strong perinuclear appearance (Figure 10b). In kidney tissue of h-L-FABP transgenic mice, CP administration caused a positive nuclear staining for h-L-FABP in the epithelium of Bowman capsule and early (S1 and S2) segments of proximal tubules (Figure 10c). The Bz + CP-treated mice showed strong cytoplasmic staining in proximal tubules of the deep cortex (S3 segment; Figure 10d). Glomeruli and distal nephron segment were mainly negative.

Morphologic changes of kidneys from h-L-FABP transgenic mice after CP treatment with and without Bz pretreatment. CP-treated h-L-FABP transgenic mice showed severe tubular necrosis in the outer cortex (primarily S1 and S2 segments of proximal tubule). Necrosis was accompanied by loss of brush border; tubular dilatation, and numerous casts (Figure 11a). Necrosis was markedly reduced in h-L-FABP transgenic animals, which were pretreated with Bz before CP administration (Figure 11b). Proximal tubules in the corticomedullary junction (primarily S3 segments of proximal tubule) were dilated, contained periodic acid-Schiff (PAS)-positive proteinous casts, and their cytoplasm was filled with PAS-positive droplets (Figure 11c). Few animals showed signs of mild to rarely moderate degree of necrosis and tubular dilatation, loss of brush border, cast formation, which were occasionally present in the outer cortex. Proximal tubules in the corticomedullary junction had no signs of dilatation, loss of brush border, and cast formation. The PAS-positive droplets present in the CP-treated mice were missing after Bz pretreatment (Figure 11d). Interstitial inflammation, edema, red blood cell extravasation, or distal nephron segment damage were not seen. Morphologic changes were quantified and the results are shown in Figure 11e.

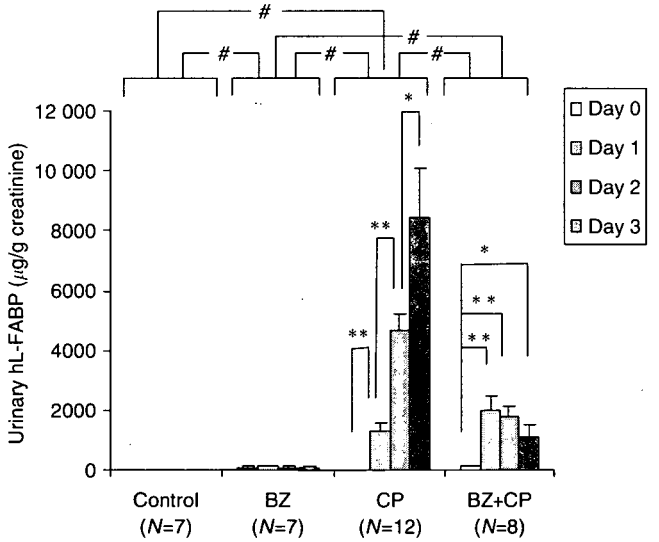

Figure 9 | Effect of BZ on urinary h-L-FABP levels after single dose of CP. Urinary h-L-FABPlevels were measured at days 1, 2, and 3 after saline control (NS)-, CP (CP)-, CP + BZ (CP + BZ)-, or saline + Bz (BZ)-treated mice by enzyme-linked immunosorbent assay as described in Materials and Methods. * Represents $P<0.05$ when urinary h-L-FABP levels were compared at day 3 and day 2 after CP administration. ** Represents $P<0.05$ when urinary h-L-FABP levels were compared at day 2 versus day 1 and day 0, and # represents $P<0.05$ when urinary h-L-FABP levels were compared among all the four groups. Bars correspond to mean ± s.e. of at least seven independent experiments under each condition.

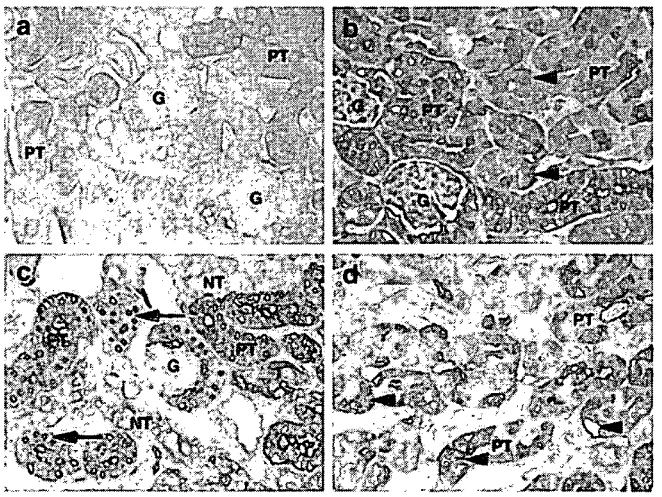

Figure 10 | Immunolocalization of h-L-FABP in h-L-FABP transgenic mice. (**a**) There was no positive immunoreactivity for h-L-FABP in kidneys from control C57Bl wild-type non-transgenic mice. (**b**) Untreated h-L-FABP transgenic animals showed strong positive staining in the cytoplasm of early (S1 and S2) segments of proximal tubules (PT). (**c**) CP administration caused a positive nuclear staining for h-L-FABP in the epithelium of Bowman capsule and early (S1 and S2) segments of proximal tubules (PT) (arrows). (**d**) The Bz + CP-treated mice showed strong cytoplasmic staining in proximal tubules (PT) of the deep cortex (S3 segment) (arrows). Glomeruli (G) and distal nephron segment were mainly negative.

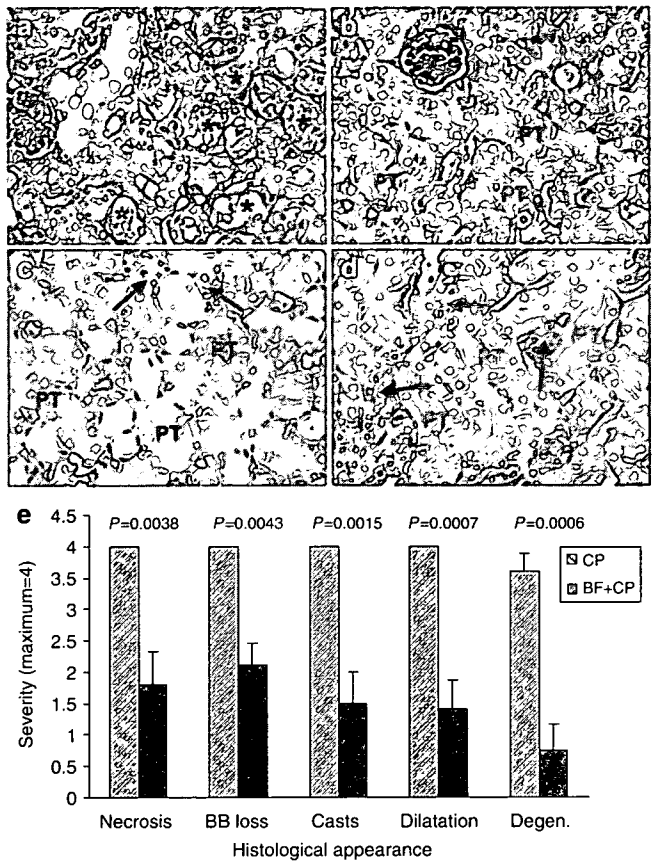

Figure 11 | Effect of Bz on kidney morphology in h-L-FABP transgenic mice after single dose of CP. Kidney morphology of h-L-FABP transgenic mice after 72 h of (**a** and **c**) CP exposure and after treatment with (**b** and **d**) Bz + CP. Severe tubular necrosis was seen in the proximal tubules (S1 and S2) of the outer cortex of (**a**) CP-treated mice (*). Bz significantly ameliorated necrosis of proximal tubules (PT) caused by (**b**) CP injection. Proximal tubules of the deep cortex (S3 segment) (PT) showed PAS-positive droplet accumulation in their cytoplasm in (**c**) CP-treated mice (arrows), which was ameliorated by (**d**) Bz pretreatment (arrows). (**e**) Quantitative evaluation of morphologic kidney damage of h-L-FABP transgenic mice after CP and Bz + CP. Values are expressed as relative severity on a scale from 0 to 4 and represent mean ± s.e. of kidney sections from at least eight mice for each experimental condition. Morphology was scored according to proximal tubule necrosis (Necrosis), brush border loss (BB Loss), cast formation within tubules (Casts), tubule dilation (Dilatation), and tubular degeneration (Degen). Statistically significant differences ($P < 0.05$) are indicated.

DISCUSSION

In this study, we demonstrate that CP causes a significant reduction in the peroxisome population of the proximal tubule determined by reduced protein expression of PMP70, and by quantification of peroxisomes using quantum dot technique. Our findings in the CP model of ARF are in agreement with findings described in the ischemia–reperfusion model of ARF, where a significant loss of catalase and fatty acid β-oxidation enzymes were accompanied by reduced number of peroxisomes in kidney tissue.[26] The mechanisms responsible for the degradation of peroxisomal proteins during ARF are unclear, but could involve autophagy, a global process by which intracellular components including soluble proteins and organelles, are degraded in lysosomes.[27–29] The presence of lysosomes containing microautophagic vacuoles has been reported previously in rat proximal tubules of animals treated with vinblastine;[30] however, the pathogenic role of these structural alterations in CP-mediated ARF remains to be defined.

Our studies showing a PPARα ligand-like fibrate increases the expression of peroxisomal proteins in mouse kidney tissue suggest that the presence of increased peroxisome proliferation in the proximal tubule is associated with cytoprotection. Peroxisome proliferation can also be seen in liver tissue of rats treated with hypolipidemic drugs such as fibrates, and it is accompanied by increased FAO.[31] Peroxisomes are organelles bound by a single membrane that are involved in metabolic processes including peroxide-based respiration, oxidative degradation of fatty acids and purines, and synthesis of plasmalogen and bile acids.[32,33] FAO is an important source of energy, especially during fasting, diabetes, or ARF.[34] Although mitochondria are considered the primary site for β-oxidation of fatty acid for energy utilization, it is now well established that peroxisomes play a key role in the metabolism of a variety of lipids such as very long-chain fatty acids, branched-chain fatty acids, dicarboxylic acids, prostaglandins, leukotrienes, thromboxanes, and pristanic acid.[35] In addition, the functional importance of peroxisomes is underscored by the severity of peroxisomal disorders such as Zellweger syndrome, X-linked adrenoleukodistrophy, and Refsum disease.[36]

Role of L-FABP in CP-induced ARF

Our study is the first one to examine the role of L-FABP in the model of CP-induced ARF. The family of fatty acid-binding proteins, which was initially discovered in 1972[37] is composed of small cytosolic proteins that are part of a conserved multigene family of intracellular lipid-binding proteins with molecular masses around 15 kDa. Two distinct isoforms of FABPs are expressed in kidney tissue the heart isoform, which is expressed in distal tubules and the liver (L-FABP) isoform, which is expressed in the proximal tubule.[38] FABPs are involved in the transport of free fatty acids from the plasma membrane to sites for oxidation (mitochondria and peroxisomes), sites for esterification into triacylglycerols or phospholipids, and the nucleus for gene regulation. Liver-type FABP found in kidney proximal tubules binds with other hydrophobic molecules such as lysophospholipids, eicosanoids, bile acids, bilirubin, heme, and hypolipidemic drugs,[39–41] and thus protects cellular structures from damage by an excess of these amphipatic molecules. Early studies by Gordon *et al.*[8] using transgenic mice to map *cis*-acting elements in the L-FABP gene indicated that nucleotides −4000 to +21 of mL-FABP contain orientation-independent suppressor sequences, which can make L-FABP to remain silent for at least the first year of postnatal life in renal proximal tubular cells of Sprague–Dawley rats and C57Bl/6 mice. We find that although L-FABP mRNA levels were slightly elevated in kidney tissue of CP-treated sv129 mice,

L-FABP protein was not found increased in kidney tissue of wild-type sv129 mice by either Western blot analysis or immunohistochemical studies. In contrast, treatment with fibrate significantly increased the expression of L-FABP protein when compared with untreated mice, and L-FABP was predominantly localized in the proximal tubule of sv-129 wild-type mice, and absent in PPARα null mice, demonstrating that the increased expression of L-FABP in kidney tissue of sv129 depends on having an intact PPARα gene.

Our studies using h-L-FABP transgenic mice to examine the pathophysiologic mechanisms involved in CP-induced ARF did allow us to uncover some important observations, which were not readily apparent when we examined kidney tissue of sv129 mice exposed to CP. The first one is that CP causes a translocation of h-L-FABP protein from the cytosolic to the nuclear compartment of proximal tubules, as shown by our immunohistochemistry studies. The effects of CP in the cellular localization of h-L-FABP could not be studied in sv129 mice because these mice do not express significant amounts of L-FABP protein. It is unclear at the moment the mechanisms that could account for the observed changes in cellular localization of h-L-FABP during CP treatment; however, future studies using immunoprecipitation and/or immunofluorescence localization using either intact kidney tissue of h-L-FABP transgenic mice or proximal tubules derived from these mice could provide additional information regarding the cellular processes and potential protein(s) involved in the regulation and/or cellular translocation of h-L-FABP during proximal tubule cell injury.

Second important observation in h-L-FABP transgenic mice was that h-L-FABP protein was shed into the urinary space early in the course of CP-induced kidney injury. Our studies using enzyme-linked immunosorbent assay methods to measure h-L-FABP protein levels allowed us to detect early shedding of h-L-FABP during the first 24 h of CP exposure, which precedes the rise on serum BUN and creatinine not detected until after 48–72 h of CP exposure. These studies suggest that shedding of h-L-FABP could represent an early urine biomarker of CP-mediated nephrotoxicity. Recently Dr Noiri and Dr Sugaya from the University of Tokyo using the model of human kidney transplantation, and more recently h-L-FABP transgenic mice and the model of 30-min ischemia–reperfusion injury demonstrated that reduced pericapillary blood flow detected by intravital CCD system was closely correlated with ischemic time of transplanted kidney. Interestingly, these investigators also detected the translocation of h-L-FABP protein from the cytoplasm of the proximal tubule to the tubular lumen by immunohistochemistry.[13] The mechanisms by which h-L-FABP is shed into the urinary space are currently unknown, but could involve disruption by CP of proximal tubule endocytic mechanisms via megalin receptor. A recent study documented that L-FABP is localized to the lysosomal compartment of the proximal tubule, but also reabsorbed from the glomerular filtrate via megalin receptor-mediated endocytosis.[9] In addition, studies using kidney-specific megalin receptor knockout mice suggest that other lipid-binding proteins such as apolipoprotein M, which is also reabsorbed in the proximal tubule via megalin receptor-mediated endocytosis, is also shed into the urinary space.[42] Our most recent findings of increased shedding of apolipoprotein M in mice that received CP suggest that disruption of megalin receptor-mediated endocytosis by CP could represent one of the mechanisms by which h-L-FABP protein and other lipocalins could be shed into the luminal space during ARF.

Third important observation made in h-L-FABP transgenic mice was that fibrate pretreatment prevented CP-mediated shedding of urinary h-L-FABP, CP-mediated translocation of proximal tubule h-L-FABP from the cytosol to the nuclear compartment, and also significantly ameliorated CP-induced acute kidney failure by reducing necrosis, brush border loss, and other parameters of proximal tubule cell injury. The increased cytosolic localization of h-L-FABP in proximal tubules of fibrate-treated mice is consistent with recent observations made in Sprague–Dawley rats treated with fibrates, where the authors demonstrated the presence of L-FABP in the matrix of liver peroxisomes.[5] The induction of peroxisomal L-FABP in rat liver tissue was accompanied by increased binding to oleic acid and cisparinaric acid, and increased β-oxidation of palmitoyl CoA and acyl CoA esterase activity, indicating that this protein modulates the function of peroxisomal lipid-metabolizing enzymes.

Altogether, our results underscore the participation of peroxisomes in the pathophysiology of CP-mediated nephrotoxicity, and the protective role of their induction via fibrates in limiting proximal tubule cell death and organ dysfunction. However, it is difficult to dissect out a single role of peroxisomes in the prevention of CP-mediated organ dysfunction, since fibrates via PPARα activation induce not only peroxisomal proteins, but also affect the transcription of other genes such as those of mitochondrial and microsomal enzymes as well. Furthermore, our previous studies also suggest a protective role of PPARα ligands on renal function by preventing not only inflammation,[19] but also by reducing systemic and renal alterations in glucose and lipid metabolism caused by CP.[23] In summary, our studies show that fibrate-mediated amelioration of CP-induced ARF is accompanied by both peroxisome proliferation as well as an increased expression of cytosolic L-FABP in the proximal tubule. The finding of an increased shedding of urinary h-L-FABP before serum creatinine rises suggests that h-L-FABP could be considered as an early biomarker of CP-mediated acute kidney injury.

MATERIALS AND METHODS

Animal model of CP-induced ARF

Experimental ARF was induced in 8-to 10-week-old male mice (strain Sv129) using CP administration. The animals used in these studies (IACUC protocol no. 2-03-1) were housed at the Veterinary Medical Unit (Central Arkansas Veterans Health Care System, Little Rock, AR, USA). When appropriate, animals were painlessly killed according to methods of euthanasia approved by the Panel on Euthanasia of the American Veterinary Medical Association. The

group of sv129 mice used for these experiments were maintained on standard chow and as indicated, a group of animals was fed with a special diet containing fibrate compound WY-14643 (WY) (1% wt/wt) for 7 days before the induction of ARF. CP was administered to sv129 mice by a single intraperitoneal injection of 20 mg/kg body weight. Engineering of h-L-FABP transgenic mice has been detailed elsewhere.[24] Briefly, genomic DNA of h-L-FABP, including its promoter region (13 kb) was microinjected into fertilized eggs obtained from C57/BL6 and CBA mice; ICR mice were used as transfected-egg recipients. The resultant transgenic mice were backcrossed for more than nine generations onto C57/BL6 mice to obtain homozygous mutant mice on an inbred background. Only heterozygous h-L-FABP transgenic mice were used in this experiment. Male h-L-FABP transgenic mice weighing 25–30 *g* were fed with standard chow diet or with a special diet containing Bz (0.5% wt/wt) for 7 days before the induction of ARF. CP was administered by a single intraperitoneal injection of 20 mg/kg body weight. After the induction of renal failure, the animals were returned to their cages and allowed free access to food and water. H-L-FABP transgenic mice were kept in glass-shielded metabolic cages (Metabolica; Sugiyamagen, Tokyo, Japan) until killing, and urine was serially collected at each 24 h interval. To measure changes in creatinine and BUN, blood was drawn from each tail vein at 0, 24, 48, and 72 h after CP administration. Serum creatinine was measured using a combined enzymic-Jaffe method.[42]

Real-time quantitative reverse transcriptase-polymerase chain reaction analysis

Mice were killed following previously described experimental conditions, and the kidneys were rapidly snap-frozen in liquid nitrogen and stored at −75°C. Total RNA was extracted with TRIzol Reagent (Invitrogen Corporation, Carlsbad, CA, USA) according to the manufacturer's directions. Total RNA extract was treated with RQ1 RNase-free DNase (Promega Corporation, Madison, WI, USA) before reverse transcription. Reverse transcription reaction was performed at 42°C for 50 min in a total volume of 20 μl containing 1 μg RNA, 0.5 μg of oligo $(dT)_{12-18}$, 200 U of superscript II RNase H reverse transcriptase (Invitrogen Life Technologies). Subsequently, reverse transcriptase was inactivated by incubation at 70°C for 15 min, followed by treatment with RNase H at 37°C for 30 min. Real-time polymerase chain reaction was performed using a DNA Engine OPTICON 2 continuous fluorescence detector (MJ Research Inc., Waltham, MA, USA) with SYBR Green I technology. In each experiment, triplicates of 50 ng cDNA (total RNA equivalent) of samples were amplified in a 50 μl reaction containing 1 × iQ™ SYBR Green Supermix (Bio-Rad Laboratories, Hercules, CA, USA). The real-time polymerase chain reaction conditions are 1 cycle at 50°C for 2 min followed by 1 cycle at 95°C (10 min); 40 cycles at 95°C (15 s), 61°C (25 s), and 72°C (16 s). Specificity of the amplified product was confirmed by melting curve analysis. For relative quantification, a standard curve was generated from a six-step cDNA dilution series. Samples were amplified with primers for mL-FABP and 28 s rRNA. The relative expression of mL-FABP and 28 s rRNA were calculated from the standard curve. Relative quantity was calculated by the ratio of mL-FABP and the appropriate 28 s rRNA expression. The primer sequences in the real time reverse transcriptase-polymerase chain reaction were for mL-FABP 5′-CATCAAAAGAGCCTGGGAAC-3′ (forward), 5′-ACACCCATACG CCAACTCTT-3′ (reverse) and 28 s rRNA 5′-AACGGCGGGAG TAACTATGA-3′ (forward), 5′-TAGGGACAGTGGGAATCTCG-3′ (reverse).

Immunoblotting

Kidney tissue was homogenized in lysis buffer (50 mM Tris (pH 7.4), 100 mM NaCl, 2.5 mM ethylenediaminetetraacetic acid, 1% Triton X-100, 0.5% NP-40, 2.5 mM Na_3VO_4, 1 mM phenylmethylsulfonyl fluoride, 25 μg/ml aprotinin and leupeptin, and 50 μg/ml Soybean trypsin inhibitor) and sonicated briefly for 10 s subsequently centrifuged at 11 000 *g* for 10 min at 4°C, and the supernatant was collected. Protein concentration was measured using the protein assay kit (Bio-Rad Laboratories). Supernatants containing 50 μg of protein were separated on a 12% sodium dodecylsulfate-polyacrylamide gel electrophoresis and then electroblotted to a nitrocellulose membrane. The membrane was blocked for 1 h with 5% nonfat dried milk in TBS-T buffer (20 mM Tris, pH 7.6, 100 mM NaCl, 0.1% Tween 20). The primary antibodies used in our studies included polyclonal L-FABP antibody (Hycult Biotechnology, Uden, The Netherlands); rabbit anti-PMP70 antibody (Affinity Bioreagents, Golden, CO, USA), and rabbit polyclonal catalase antibody (Calbiochem, San Diego, CA, USA). These antibodies were used at a 1:1000 dilution and membranes were incubated overnight in TBS-T buffer containing 5% nonfat dried milk at room temperature. After washing three times with TBS-T buffer, the membranes were incubated with a horseradish peroxidase-conjugated goat anti-rabbit IgG as a second antibody (1:5000 dilution) for 1 h at room temperature. Proteins were visualized using by enzyme-linked enhanced chemiluminescence (Amersham, Arlington Heights, IL, USA). The membranes were stripped and then probed with β-actin antibodies (Chemicon, Temecula, CA, USA) as an internal control. Signals on the blots were visualized by autoradiography and quantitated by densitometry using ImageQuant image analysis system (Storm Optical Scanner; Molecular Dynamics, Sunnyvale, CA, USA).

Tissue preparation for immunohistochemistry

Kidney tissue samples were obtained from control-, WY-, CP-, and WY + CP-treated sv129 mice, and control-, CP-, Bz-, and Bz + CP-treated h-L-FABP transgenic mice. Tissues were fixed in 10% neutral-buffered formalin and embedded in paraffin. Sections (6 μm) were placed on silane-coated slides (Sigma, St Louis, MO, USA) and processed for morphologic analysis immunohistochemical localization of PMP-70, L-FABP, and for immunofluorescent staining of peroxisomes.

Morphologic analysis

Kidney sections were stained with PAS and the degree of morphologic damage was determined using light microscopy. The following parameters were graded to assess morphological damage after CP and Bz + CP treatment: brush border loss, red blood cell extravasation, tubular dilatation, tubular degeneration, tubular necrosis, tubular cast formation, interstitial edema, and inflammation. These parameters were evaluated on a scale of 0–4, which ranged from not present (0), mild (1), moderate (2), severe (3), and to very severe (4). Each parameter was determined at least on eight different animals. Statistical significance was assessed by the two-sided Student's *t*-test for independent samples.

PMP70 and L-FABP immunohistochemistry

To further ascertain that CP or fibrate affect the expression of PMP70, we performed immunostaining of mouse kidney tissue treated with CP or fibrate using a rabbit anti-PMP70 antibody (1:500 dilution; Affinity Bioreagents). In addition, since our Western blot analysis suggested that fibrate increased the expression of

L-FABP protein, we also performed immunostaining of mouse kidney tissue using a L-FABP polyclonal antibody that recognized mL-FABP (1:100 dilution; Hycult Biotechnology, Uden, The Netherlands), after which goat biotinylated anti-rabbit antibody (Vector Laboratories Inc., Burlingame, CA, USA) and ABC Elite Vectastain Kit (Vector Laboratories Inc.) was used. Nonspecific staining was blocked with 5% normal goat serum (Sigma), and the sections were permeabilized with 0.1% Triton X-100 (Sigma) and 0.05% saponin (Sigma) digestion. Endogenous peroxidase was inactivated with 1% hydrogen peroxide in phosphate-buffered saline/methanol (1:1).

Immunofluorescent staining of peroxisomes

To examine the effect of fibrate and CP on peroxisome proliferation in kidney tissue, we used a novel method of immunofluorescent labeling of peroxisomes, using an antibody to the PMP70, coupled with fluorescent nanocrystals, Quantum Dots.[24] This method is applicable to standard formalin-fixed and paraffin-embedded tissues. Paraffin sections were deparaffinized and hydrated in graded alcohol series and distilled water. Endogenous biotin sites were blocked by avidin/biotin blocking Kit (Vector Laboratories Inc.) according to the manufacturer's instructions. Nonspecific staining was blocked with 10% normal goat serum. The sections were incubated with rabbit anti-PMP70 antibody (diluted 1:500 in 10% normal goat serum; Affinity Bioreagents) for 1 h, then washed in phosphate-buffered saline and incubated for 30 min with (1:1000 dilution in phosphate-buffered saline) biotinylated goat anti-rabbit IgG (Sigma). After washing three times in phosphate-buffered saline, they were incubated with (1:100 dilution) 605 nm streptavidin-coated Quantum Dots (Quantum Dot Corp., Hayward, CA, USA). The sections were coverslipped and counterstained using mounting media containing 4,6-diamidino-2-phenylindole (Vector Laboratories Inc.). Fields for microscopic evaluation and subsequent image analysis were selected randomly. Fluorescent images were captured on a Zeiss LSM410 confocal microscope using a plan-apochromat $\times 63$ oil immersion objective with 1.4 numerical apertures. Blue, green, and red images were captured separately and overlaid. 4,6-Diamidino-2-phenylindole and quantum dot 605 fluorophores were excited with a 405 diode laser. Red-orange emitted light was detected after filtering with a 590–610 nm band pass filter, 4,6-diamidino-2-phenylindole-emitted light was filtered with a 435–485 nm band pass filter (D460/50m; Chroma Technology Corporation., Rockingham, VT, USA), and green auto-fluorescence was filtered through a 500–550 nm band pass filter (HQ525/50m; Chroma). The pixel density of the quantum dot signals were analyzed by Image J Software. Eight microscopic fields corresponding to the cortex area on pairs of adjacent sections (four microscopic fields/sections) from each animal kidney were chosen for area imaging in each treatment group. We quantified the pixel intensity of only orange/red color of quantum dot signals.

Measurement of urinary h-L-FABP protein

The enzyme-linked immunosorbent assay method for measuring urinary h-L-FABP was reported previously.[25,43,44] H-L-FABP protein standard or 50 μl of urine samples obtained from h-L-FABP transgenic mice are first treated with a pretreatment solution, and then transferred into a 96-well plate coated with a monoclonal antibody against h-L-FABP. After 1 h incubation, the wells are washed and then the conjugate reagent is added as secondary antibody for another hour allowing the binding of the h-L-FABP antigen, the immobilized antibody and the conjugate antibody. After incubation, the plate is washed and a substrate solution for the immunoperoxidase reaction is added for 30 min to develop a color based on the amount of h-L-FABP antigen present in the samples. h-L-FABP concentration is measured by measuring the absorbance of each well at 492 nm and calculated mass is determined based on a calibration curve. Urinary h-L-FABP levels is expressed as the ratio of the urinary h-L-FABP in micrograms to the urinary creatinine level (mg).

ACKNOWLEDGMENTS

This work was supported by National Institutes of Health Grant PO-1 DK 58324-01A5 and a VA Merit Award to Dr Didier Portilla. We acknowledge Dr Renu Bhatt for her technical help with the peroxisomal staining using quantum dots technique. A part of this study was supported by grants from the Health and Labour Science Research Grants for Research on Human Genome, Tissue Engineering, and Food Biotechnology from the Ministry of Health, Labour and Welfare of Japan (KN, EN, TS) and MEXT Leading Project (03023168) in Japan (EN).

REFERENCES

1. Chmurzynska A. The multigene family of fatty acid-binding proteins (FABPs): function, structure and polymorphism. *J Appl Genet* 2006; **47**: 39–48.
2. Zimmerman AW, Veerkamp JH. New insights into the structure and function of fatty acid-binding proteins. *Cell Mol Life Sci* 2002; **59**: 1096–1116.
3. Haunerland NH, Spener F. Fatty acid binding proteins – insights from genetic manipulations. *Prog Lipid Res* 2004; **43**: 328–349.
4. Huang H, Starodub O, McIntosh A *et al.* Liver fatty acid-binding protein colocalizes with peroxisome proliferator activated receptor-α and enhances ligand distribution to nuclei of living cells. *Biochemistry* 2004; **43**: 2484–2500.
5. Antonenkov VD, Sormunen RT, Ohlmeier S *et al.* Localization of a portion of the liver isoform of fatty acid-binding protein (L-FABP) to peroxisomes. *Biochem J* 2006; **394**: 475–484.
6. Reddy JK. Peroxisome proliferators and peroxisome proliferators-activated receptor-α. *Am J Pathol* 2004; **164**: 2305–2321.
7. Kaikaus RM, Chan WK, Ortiz de Montellano PR *et al.* Mechanisms of regulation of liver fatty acid-binding protein. *Mol Cell Biochem* 1993; **123**: 93–100.
8. Simon TC, Roth KA, Gordon JI. Use of transgenic mice to map cis-acting elements in the liver fatty acid-binding protein gene (Fabpl) that regulate its cell lineage-specific, differentiation-dependent, and spatial patterns of expression in the gut epithelium and in the liver acinus. *J Biol Chem* 1993; **268**: 18345–18358.
9. Oyama Y, Takeda T, Hama H *et al.* Evidence for megalin-mediated proximal tubular uptake of L-FABP, a carrier of potentially nephrotoxic molecules. *Lab Invest* 2005; **85**: 522–531.
10. Maatman RGHJ, Van de Westerlo EMA, Van Kuppevelt THMSM *et al.* Molecular identification of the liver- and the heart-type fatty acid-biding proteins in human and rat kidney. *Biochem J* 1992; **288**: 285–290.
11. Maatman RGHJ, Van Kuppevelt THMSM, Veerkamp JH. Two types of fatty acid-binding protein in human kidney. Isolation, characterization and localization. *Biochem J* 1991; **273**: 759–766.
12. Kamijo A, Sugaya T, Hikawa A *et al.* Urinary excretion of fatty acid-binding protein reflects stress overload on the proximal tubules. *Am J Pathol* 2004; **165**: 1243–1255.
13. Sugaya T, Noiri E, Yamamoto T *et al.* L-Type fatty acid-binding protein ameliorates renal ischemia reperfusion injury in human L-FABP transgenic mice. *Nephrology* 2005; **10**(Suppl): A133.
14. Portilla D, Dai G, Peters JM *et al.* Etomoxir-induced PPARalpha modulated enzymes protect during acute renal failure. *Am J Physiol Renal Physiol* 2000; **278**: F667–F675.
15. Portilla D, Dai G, McClure T *et al.* Alterations of PPARalpha and its coactivator PGC-1 in CP-induced acute renal failure. *Kidney Int* 2002; **62**: 1208–1218.
16. Portilla D. Energy metabolism and cytotoxicity. *Semin Nephrol* 2003; **23**: 432–438.
17. Li S, Wu P, Yarlagadda P *et al.* PPARalpha ligand protects during CP-induced acute renal failure by preventing inhibition of renal FAO and PDC activity. *Am J Physiol Renal Physiol* 2004; **286**: F572–F580.

18. Li S, Bhatt R, Megyesi J *et al.* PPAR-alpha ligand ameliorates acute renal failure by reducing CP-induced increased expression of renal endonuclease G. *Am J Physiol Renal Physiol* 2004; **287**: F990–F998.
19. Li S, Gokden N, Okusa MD *et al.* Anti-inflammatory effect of fibrate protects from CP-induced ARF. *Am J Physiol Renal Physiol* 2005; **289**: F469–F480.
20. Nagothu KK, Bhatt R, Kaushal GP *et al.* Fibrate prevents CP-induced proximal tubule cell death. *Kidney Int* 2005; **68**: 2680–2693.
21. Schonefeld M, Noble S, Bertorello AM *et al.* Hypoxia-induced amphiphiles inhibit renal NaK-ATPase. *Kidney Int* 1996; **49**: 1289–1296.
22. Feldkamp T, Kribben A, Roeser NF *et al.* Accumulation of nonesterified fatty acids causes the sustained energetic deficit in kidney proximal tubules after hypoxia-reoxygenation. *Am J Physiol Renal Physiol* 2005; **290**: F465–F477.
23. Portilla D, Li S, Nagothu KK *et al.* Metabolomic study of CP-induced nephrotoxicity. *Kidney Int* 2006; **69**: 2194–2204.
24. Colton HM, Falls JG, Ni H *et al.* Visualization and quantitation of peroxisomes using fluorescent nanocrystals: treatment of rats and monkeys with fibrates and detection in the liver. *Toxicol Sci* 2004; **80**: 183–192.
25. Kamijo A, Sugaya T, Hikawa A *et al.* Urinary excretion of fatty acid-binding protein reflects stress overload on the proximal tubules. *Am J Pathol* 2004; **165**: 1243–1255.
26. Gulati S, Singh AK, Irazu C *et al.* Ischemia-reperfusion injury: biochemical alterations in peroxisomes of rat kidney. *Arch Biochem Biophys* 1992; **295**: 90–100.
27. Klionsky DJ. The molecular machinery of autophagy: unanswered questions. *J Cell Sci* 2005; **118**: 7–18.
28. Cuervo AM. Autophagy in neurons: it is not all about food. *Trends Mol Med* 2006; **12**: 461–464.
29. Dunn WA, Cregg JM, Kiel J AKW *et al.* Pexophagy. The selective autophagy of peroxisomes. *Autophagy* 2005; **1**: 75–83.
30. Berkenstam A, Ahlberg J, Glaumann H. Isolation and characterization of autophagic vacuoles from rat kidney cortex. *Virchows Arch B Cell Pathol Incl Mol Pathol* 1983; **44**: 275–286.
31. Schrader M, Fahimi HD. Peroxisomes and oxidative stress. *Biochimica et Biophysica Acta* 2006; **1763**: 1755–1766.
32. Wanders RJ, Waterham HR. Biochemistry of mammalian peroxisomes revisited. *Annu Rev Biochem* 2006; **75**: 295–332.
33. Rottensteiner H, Theodoulou FL. The ins and outs of peroxisomes: coordination of membrane transport and peroxisomal metabolism. *Biochimica et Biophysica Acta* 2006; **1763**: 1527–1540.
34. Visser WF, van Roermund CWT, Ijlst L *et al.* Metabolite transport across the peroxisomal membrane. *Biochem J* 2007; **401**: 365–375.
35. Wanders RJ, van Roermund CW, Visser WF *et al.* Peroxisomal fatty acid α and β-oxidation in health and disease: new insights. *Adv Exp Med Biol* 2003; **544**: 293–302.
36. Ockner RK, Manning JA, Poppenhausen RB *et al.* A binding protein for fatty acids in cytosol of intestinal mucosa, liver, myocardium, and other tissues. *Science* 1972; **177**: 56–58.
37. Maatman RG, van den Westerlo EM, van Kuppevelt TH *et al.* Molecular identification of the liver and the heart-type fatty acid binding proteins in human and rat kidney. Use of the reverse transcriptase polymerase chain reaction. *Biochem J* 1992; **15**: 285–290.
38. Vancura A, Haldar D. Regulation of mitochondrial and microsomal phospholipid synthesis by liver fatty acid binding protein. *J Biol Chem* 1992; **267**: 14353–14359.
39. Raza H, Pongubala JR, Sorof S. Specific high affinity binding of lipooxygenase metabolites of arachidonic acid by liver fatty acid-binding protein. *Biochem Biophys Res Commun* 1989; **161**: 448–455.
40. Takikawa H, Kaplowitz N. Binding of bile acids, oleic acid, and organic anions by rat and human hepatic Z protein. *Arch Biochem Biophys* 1986; **251**: 385–392.
41. Faber K, Hvidberg V, Moestrup SK *et al.* Megalin is a receptor for apolipoprotein M, and kidney-specific megalin-deficiency confers urinary excretion of apolipoprotein M. *Mol Endocrinol* 2006; **20**: 212–218.
42. Masson P, Ohlsson P, Bjorkhem I. Combined enzymic-Jaffe method for determination of creatinine in serum. *Clin Chem* 1981; **27**: 18–21.
43. Kamijo A, Kimura K, Sugaya T *et al.* Urinary fatty acid-binding protein as a new clinical marker of the progression of chronic renal disease. *J Lab Clin Med* 2004; **143**: 23–30.
44. Kamijo-Ikemori A, Sugaya T, Obama A *et al.* Liver-type fatty acid-binding protein attenuates renal injury induced by unilateral ureteral obstruction. *Am J Pathol* 2006; **169**: 1107–1117.

Original Paper

nephron
Experimental
Nephrology

Nephron Exp Nephrol 2008;108:e19–e26
DOI: 10.1159/000112912

Received: July 11, 2007
Accepted: October 24, 2007
Published online: January 8, 2008

Urinary Human L-FABP Is a Potential Biomarker to Predict COX-Inhibitor-Induced Renal Injury

Tamami Tanaka[a] Eisei Noiri[a, d] Tokunori Yamamoto[b] Takeshi Sugaya[c]
Kousuke Negishi[a] Rui Maeda[d] Kazuo Nakamura[c] Didier Portilla[e]
Momokazu Goto[b] Toshiro Fujita[a]

[a]Departments of Nephrology and Endocrinology and Hemodialysis and Apheresis, Tokyo University Hospital, Tokyo, [b]Department of Urology, Nagoya University Hospital, Nagoya, [c]CMIC Co. Ltd., Tokyo, and [d]Center for NanoBio Integration, University of Tokyo, Tokyo, Japan; [e]Division of Nephrology, Department of Internal Medicine, University of Arkansas for Medical Sciences and Central Veteran Healthcare System, Little Rock, Ark., USA

Key Words
Biomarker development · Chronic renal injury · Cyclooxygenase inhibitors · L-type fatty acid binding protein

Abstract
Background/Aim: A strong demand exists for the development of sensitive biomarkers in the nephrology field. We propose urinary human L-type fatty acid binding protein (L-FABP) as an earlier biomarker to detect the outcome of chronic renal injury induced by cyclooxygenase (COX) inhibitors using human L-FABP transgenic mice. ***Methods:*** After consuming a low-sodium diet for 2 weeks, transgenic mice were administered meloxicam or celecoxib with the low-sodium diet. Mice were sacrificed 2 days and 4 weeks after starting COX inhibitors, and urine was collected 24 and 48 h and 1, 2, 3, and 4 weeks after starting COX inhibitors. Celecoxib-treated mice were divided into responders or nonresponders according to urinary L-FABP levels, and histology, urinary L-FABP and peritubular capillary blood flow were evaluated. ***Results:*** Meloxicam-treated mice showed a higher blood pressure than control mice. Urinary L-FABP was significantly increased in COX inhibitor-treated mice. Peritubular capillary blood flow in all meloxicam-treated mice and in some celecoxib-treated mice was significantly decreased. Although blood urea nitrogen was not increased, interstitial fibrosis and macrophage infiltration were revealed, especially in meloxicam-treated mice. Responders showed an increase of fibrotic areas and correlations between urinary L-FABP and peritubular capillary blood flow. ***Conclusion:*** Urinary L-FABP is capable of revealing chronic renal injury induced by COX inhibitors.

Introduction

The increasing population of geriatric individuals dictates that nonsteroidal anti-inflammatory drugs (NSAIDs) and cyclooxygenase (COX)-2 inhibitors must be prescribed more carefully because the renin-angiotensin-aldosterone system is more upregulated among older people than among younger people. Older people are often advised to reduce their sodium consumption when suffering from hypertension, diabetes mellitus, and chronic kidney disease [1, 2]. A low-sodium diet might further increase renin-angiotensin-aldosterone system activity. Moreover, the necessity of pain relief prescription medication will increase because of age-related low-

KARGER
Fax +41 61 306 12 34
E-Mail karger@karger.ch
www.karger.com

1660–2129/08/1081–0019$24.50/0

Accessible online at:
www.karger.com/nee

Eisei Noiri, MD, PhD
107 Lab., Departments of Nephrology and Endocrinology
University of Tokyo, 7-3-1 Hongo, Bunkyo
Tokyo 113-8655 (Japan)
Tel./Fax +81 3 5814 8696, E-Mail noiri-tky@umin.ac.jp

er back pain, osteoarthritis, and other causes. Most NSAIDs inhibit both COX-1 and COX-2 [3]. Selective inhibition of COX-2 is considered to be associated with most beneficial therapeutic anti-inflammatory efficacy in NSAIDs [4, 5]. Therefore, COX-2-selective inhibitors like meloxicam and a COX-2-specific inhibitor like celecoxib have been developed by pharmaceutical companies. In fact, COX-1 is constitutively expressed throughout the human body, playing crucial roles in normal gastrointestinal mucosa and platelet function. Inhibition of COX-1 is associated with nonbeneficial outcomes like gastrointestinal ulceration and only partial therapeutic efficacy because of bleeding tendencies induced by platelet dysfunction [6]. In the presence of inflammatory processes by endotoxins and cytokines, etc., COX-2 is an inducible enzyme. In the kidney, COX-2 is apparently expressed in a constitutive fashion; Cheng et al. [7] reported that the renal isoenzyme of COX-2 is capable of inhibiting renin secretion in macula densa [7] and that this decrease in renin secretion might consequently increase blood pressure and serum potassium levels and lead to edema formation and decreased glomerular filtration [8]. Therefore, the long-term aspects of the safety of COX-2 inhibitors are not yet fully understood because the exposure periods of those drugs are rather short, and inhibitors might be nephrotoxic. However, it is considerably difficult to monitor chronic nephrotoxicity and will be extremely difficult to anticipate it at an earlier time point after starting such prescriptions. This study investigates the applicability of urinary L-type fatty acid binding protein (L-FABP) to indicate potential renal damage. The dosage of the COX-2 inhibitors used for this study was nontoxic in rodents, but demonstrated different histological responses such as interstitial fibrosis after administration for 4 weeks. These effects were not detectable by a serum marker, blood urea nitrogen, but urinary L-FABP could differentiate between responders and nonresponders. Urinary L-FABP is a potential biomarker to monitor the occurrence of drug-induced nephrotoxicity during chronic treatment.

Materials and Methods

Materials

All chemical compounds were purchased from Wako Pure Chemical Industries (Osaka, Japan) unless otherwise specified. Celecoxib was provided by Pfizer (New York, N.Y., USA). Meloxicam was generously provided by Daiichi-Sankyo (Tokyo, Japan). Rat anti-mouse F4/80 macrophage antigen antibody (MCA497R) was purchased from Serotec (Raleigh, N.C., USA). All experiments were conducted in accordance with the NIH Guide for the Care and Use of Laboratory Animals [US Department of Health and Human Services, National Institutes of Health, NIH Publication No. 86-23, 1985]. The experimental protocol was qualified and approved by the Committee of Animal Resources of the University of Tokyo (No. 460).

Experimental Protocol

Before starting drug administration, the mice were fed a low-sodium diet (0.01% Na^+; Oriental Yeast, Tokyo) with water ad libitum for more than 2 weeks. This feeding pattern was continued after starting drug administration. The control group was fed a normal diet. Either meloxicam 2.5 mg/kg or celecoxib 20 mg/kg was dissolved in 0.5% carboxymethylcellulose and administered daily per os. The dosages used for both compounds were in the nontoxic range for mice based on previously published reports [9].

Measurement of Blood Pressure

The blood pressure was measured by tail cuff sensor (MK-2000; Muromachi Kikai, Tokyo) 2 weeks after feeding the low-sodium diet and 2 days and 4 weeks after starting meloxicam. The blood pressure was measured three times in each animal and averaged; the values were further averaged in each group.

Intravital CCD Video Analysis of the Peritubular Capillary Blood Flow

Renal cortical peritubular capillaries were measured 2 weeks after starting the low-sodium diet and 2 days after starting COX inhibitors. The renal cortical peritubular capillaries were viewed using a pencil-lens probe charge-coupled device video microscope with a 1-mm (diameter) tip, as previously described [10, 11]. The probe had a magnification of ×520, a depth of field <60 μm, and spatial resolution of 0.86 μm, permitting identification of individual erythrocytes. The probe was equipped with optical fibers transmitting light from a xenon AC 100-volt light source. Video signals were digitized using an analog-to-digital converter and recorded using a digital videocassette recorder (DVCAM; Sony, Tokyo) interfaced to a computer. The device (Scalar, Tokyo) used in this study was described previously [10]. The peritubular capillary blood flow was recorded by means of a pencil-lens microscope connected directly to the decapsulated renal surface. Images were recorded on digital videocassette tapes at a rate of 30 frames/s from the kidney. Animal cohorts are detailed in the Results section. Visualization of the images was improved on freeze frames using NIH Image combined with subtracting image filtering using Matlab software (The MathWorks, Natick, Mass., USA). The velocity of erythrocytes in individual segments of the peritubular capillaries, as representative of peritubular capillary flow, was analyzed using a program specifically designed for adaptation from the previously developed algorithm [12].

Human L-FABP Chromosomal Transgenic Mice

Human L-FABP transgenic mice, described previously elsewhere [13], were used for these experiments. Briefly, the genomic DNA of human L-FABP, including its promoter region (13 kb), was microinjected into fertilized eggs obtained from C57B/6 and CBA mice. We used ICR mice as the recipients of the transfected eggs. The resultant transgenic mice were backcrossed for more than nine generations onto C57B/6 mice to obtain homozygous

mutant mice on an inbred background. Only heterozygous L-FABP transgenic mice were used in this experiment. Male wild-type and L-FABP transgenic mice weighing 20–25 g were allowed food and water ad libitum. The animals were first anesthetized with a combination of ketamine hydrochloride 11.6 mg/100 g and xylazine hydrochloride 0.77 mg/100 g; then they were killed.

Measurement of Blood Urea Nitrogen

Blood urea nitrogen was measured using the urease-indophenol method (Urea NB kit; Wako Pure Chemical Industries) using a 96-well plate reader (SpectraMax; Molecular Devices, Sunnyvale, Calif., USA) and 570 nm wavelength.

Urinary N-Acetyl-β-D-Glucosaminidase (NAG)

NAG is rich in renal tubular epithelial lysosomes. An increase of NAG is the hallmark of tubular epithelial cell injury. Absorbance at 580 nm indicates the colorimetric reaction of *m*-cresol, which is generated by the hydrolytic reaction of sodio-*m*-cresolsulfonphthaleinyl with NAG [9]. This assay is commercially available; the entire process was conducted following the manufacturer's protocol (NAG test; Shionogi, Osaka).

Measurement of Human L-FABP by ELISA

Urinary and serum human L-FABP levels were measured using a sandwich ELISA kit following the manufacturer's protocol (CMIC, Tokyo). The coefficient of variation is within 10% when the intra-assay reproducibility was determined by the same sample eight times. The measurable range of this kit is between 4 and 400 ng/ml. This ELISA kit does not cross-react with murine L-FABP. Measurements were performed in duplicate.

Quantitative Evaluation of Renal Fibrosis

Formalin-fixed sections (2 μm) were stained using Masson's trichrome, which indicates fibrosis as blue. The area of interstitial fibrosis in the cortex was evaluated using the computer-aided evaluation program AIS (Fuji Photo Film, Tokyo), as described previously [14]. Viewed at ×200, ten randomly selected nonoverlapping fields ranging from the outer medulla to the cortical region were analyzed. The fibrotic areas stained in blue were depicted in digital images; then the percentage of the fibrotic area was calculated relative to the entire field area (percentage area). Glomeruli and large vessels were not included in the microscopic fields for image analyses. Scores of respective kidneys were averaged; scores of each animal were also averaged.

Immunohistochemical Analysis

Immunohistochemical staining of 2-μm paraffin sections was performed using indirect techniques. Biotin-free immunohistochemical staining using a horseradish-peroxidase-conjugated polymer system was conducted according to the manufacturer's protocols with the Histofine Simple Stain Mouse MAX-PO (Rat) kit (Nichirei, Tokyo). The deparaffinized sections were preincubated with 0.3% hydrogen peroxide for 15 min and incubated with a primary antibody overnight at 4°C, followed by polymer-conjugated anti-mouse IgG. Protease K treatment was necessary for anti-F4/80 antibody. Diaminobenzidine tetrahydrochloride (Nichirei) was used for the substrate-chromogen reaction followed by counterstaining with hematoxylin. Control sections were subjected to secondary antibody only (blank). Mounted preparations were examined under a light microscope (E600; Nikon, Tokyo). Images were captured using a CCD camera (DM-1200; Nikon). Image software AIS was also used for quantitative evaluation of F4/80-positive area.

Table 1. Effects of the different diets and meloxicam on systolic blood pressure

Diet and meloxicam	Systolic blood pressure, mm Hg
Normal diet (n = 5)	117.2 ± 2.4
Low-Na diet for 2 weeks (n = 5)	117.5 ± 4.5
Low-Na diet for 2 weeks and meloxicam for	
2 days (n = 4)	137.8 ± 6.7
4 weeks (n = 6)	153.0 ± 8.2

Statistical Analyses

Differences among experimental groups were detected using one-way ANOVA with Tukey's HSD post hoc test. Student's t test was applied to some experimental results. Values are expressed as mean ± SD; $p < 0.05$ was considered significant. Correlations between two indicators were evaluated using the Spearman rank test, and $r < 0.75$ was considered a significant correlation.

Results

Blood Pressure

The systolic blood pressure (table 1) of mice fed a normal diet (n = 5) was 117.2 ± 2.4 mm Hg, whereas that of mice fed a low-sodium diet for more than 2 weeks (n = 5) was unchanged with 117.5 ± 4.5 mm Hg. Mice administered meloxicam for 2 days on a low-sodium diet showed a significantly higher systolic blood pressure of 137.8 ± 6.7 mm Hg (n = 4, $p < 0.05$ vs. low-sodium diet alone); those that received it for 4 weeks exhibited a further increase to 153.0 ± 8.2 mm Hg (n = 6, $p < 0.05$ vs. low-sodium diet alone).

Urinary Indicators

During daily administration of meloxicam for 2 days (n = 5), urinary L-FABP adjusted by urinary creatinine was significantly increased at 24 h (98.3 ± 39.4 μg/g creatinine; $p < 0.05$ compared to the basal level of 12.8 ± 3.7 μg/g creatinine, n = 5) and was further increased at 48 h (207.3 ± 48 μg/g creatinine; $p < 0.05$ vs. basal level and vs. 24 h) (fig. 1). Serum L-FABP at the 48-hour time point was 27.8 ± 16.1 ng/ml, which was statistically indistinct from the basal level. Similar to the data for meloxicam, animals that were administered celecoxib on a low-sodium diet showed a significant increase of urinary L-

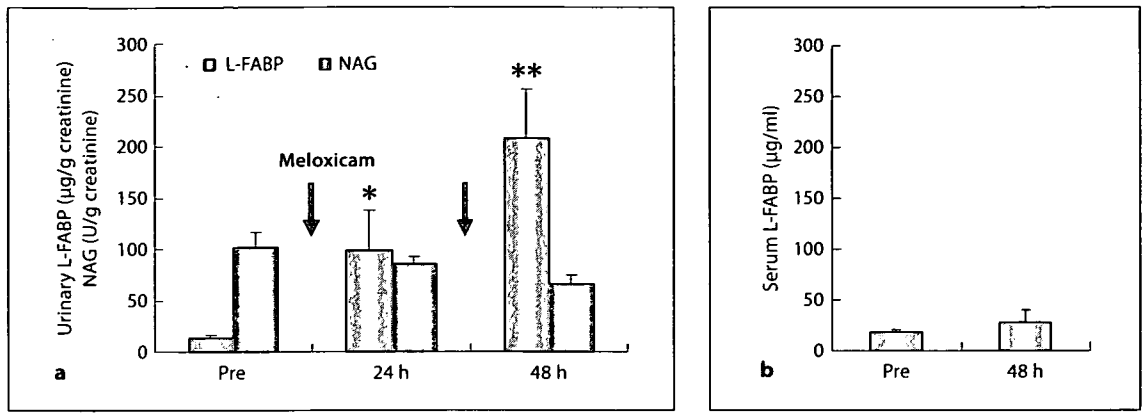

Fig. 1. Urinary L-FABP and NAG (**a**) and serum L-FABP levels (**b**). Animals were given a low-Na diet for 2 weeks before daily administration of meloxicam 2.5 mg/kg p.o. Both urinary L-FABP and NAG were standardized by urinary creatinine. * $p < 0.05$ pre vs. 24 h; ** $p < 0.05$ pre and 24 h vs. 48 h.

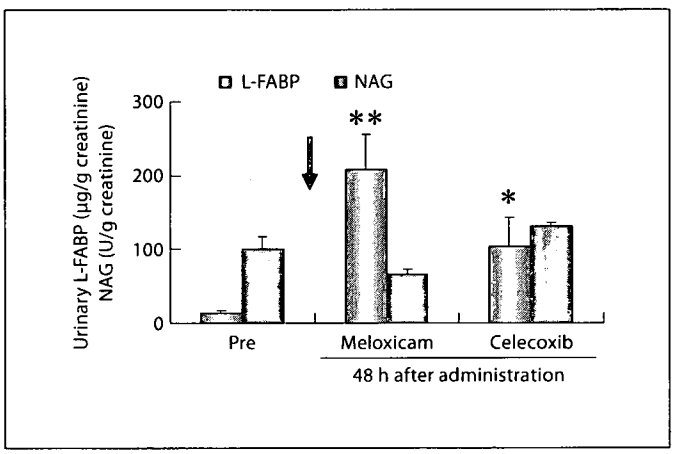

Fig. 2. Urinary L-FABP and NAG levels 48 h after starting either meloxicam or celecoxib. Animals were given a low-Na diet for 2 weeks before starting daily administration. Both urinary L-FABP and NAG were standardized by urinary creatinine. Each group includes 6 animals. * $p < 0.05$ celecoxib vs. basal level; ** $p < 0.05$ meloxicam vs. basal level or celecoxib.

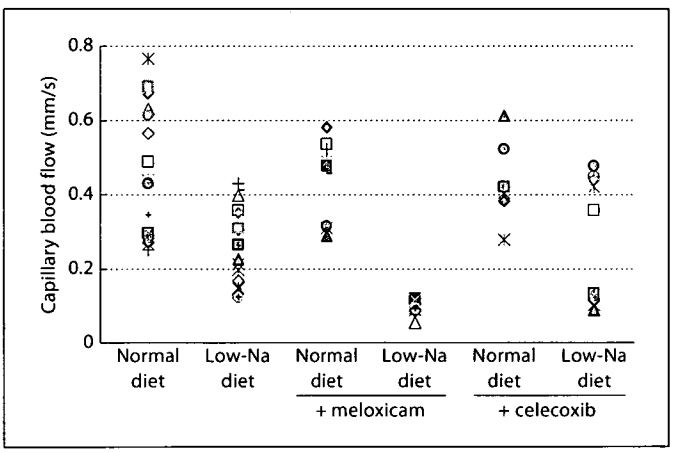

Fig. 3. Peritubular capillary blood flow measured using intravital CCD video. Low-Na diet denotes that animals were given a low-sodium diet 2 weeks before starting daily administration. Either meloxicam or celecoxib was administered for 2 days before analyses.

FABP: 103.7 ± 39.5 μg/g creatinine (fig. 2). Compared to urinary L-FABP, urinary NAG was insensitive (fig. 2).

Peritubular Capillary Blood Flow

Peritubular capillary blood flow was monitored next using an intravital CCD video system. As shown in figure 3, the peritubular capillary blood flow was reduced in the low-sodium diet group (0.27 ± 0.02 mm/s, n = 19) compared to animals fed a normal diet (0.47 ± 0.04 mm/s, n = 19), but this value did not indicate a statistically significant difference. Mice treated with either meloxicam or celecoxib showed values in between those of animals with normal and low-sodium diets. It is noteworthy that mice treated with meloxicam on a low-sodium diet showed a significant decrease of peritubular capillary blood flow (0.096 ± 0.004 mm/s, n = 19; $p < 0.05$ vs. normal diet, normal diet + meloxicam, and normal diet + celecoxib). Mice treated with celecoxib intriguingly showed a different response from that to meloxicam. Some animals showed a significant decrease of peritubu-

lar capillary blood flow compared to that of the normal-diet group, but others showed a blood flow equivalent to that of animals of the normal-diet group. Although we recently reported a significant correlation between the level of urine L-FABP and peritubular capillary blood flow [15], the observation described above reconfirmed that remarkable correlation.

Pathology

Both meloxicam and celecoxib were further administered for 4 weeks. Staining of kidneys using Masson's trichrome showed a marked increase of interstitial fibrosis in meloxicam-treated animals on a low-sodium diet compared with the animals on a normal diet (fig. 4a). Moreover, cellular infiltration into the interstitium was partially observed in meloxicam-treated animals on a low-sodium diet. Figure 4b shows results of quantitative analyses of fibrosis using image software (AIS), where the region of interest for fibrosis was preassigned in terms of the hue and contrast level. The small histological pictures shown above the bar graphs in figure 4b are representative AIS images. The total proportional area of fibrosis was significantly increased in both meloxicam-treated and celecoxib-treated animals on a low-salt diet compared with animals receiving a normal diet ($p < 0.05$, $n = 6$ in each group), although the level of fibrosis was mild to moderate. Interstitial cellular infiltration was observed at 4 weeks in kidneys harvested from meloxicam-treated animals receiving the low-sodium diet. Therefore, the F4/80 macrophage antigen antibody was applied for detection (fig. 5). The kidneys obtained from meloxicam-treated animals on a low-sodium diet showed a remarkable increase of interstitial infiltration of macrophages compared with animals receiving a normal diet ($p < 0.05$, $n = 5$ in each group). Those of the celecoxib-treated animals exhibited F4/80-positive cells at the vicinity of the peritubular region, but quantitative analyses demonstrated that the F4/80-positive staining area in celecoxib-treated animals was not as broad as that of the meloxicam-treated animals ($p < 0.05$, $n = 5$ in each group).

Blood Urea Nitrogen

The level of blood urea nitrogen at 4 weeks after administration of these preparations was not significantly altered and was similar among the animals ($n = 6$ in each group; fig. 6).

Urinary L-FABP Level and Fibrosis

Because animals treated with celecoxib on a low-sodium diet for 2 days showed different responses of peritubular capillary blood flow, depending on individual animals, we continued administration of celecoxib for 4 weeks and collected urine every week. Some animals showed increased urine L-FABP levels during 1 week after

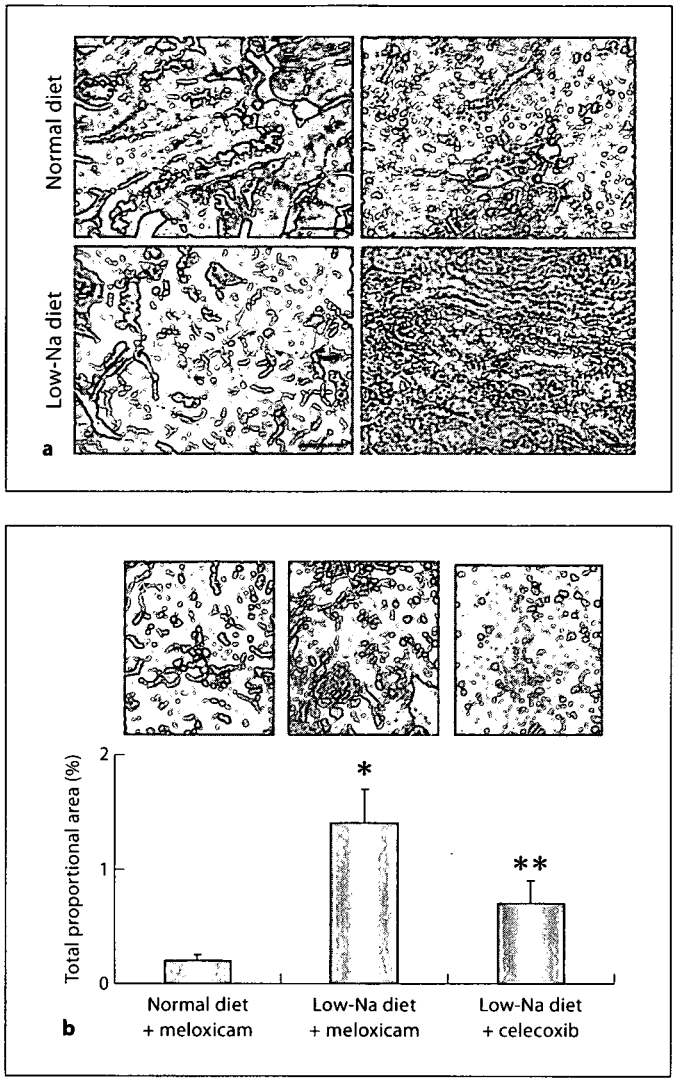

Fig. 4. a Renal histology of animals administered meloxicam for 4 weeks on either a normal or a low-Na diet. Left panels demonstrate Masson's trichrome. ×200. Right panels show periodic acid-Schiff. ×100. Blue staining in the lower left panel (Masson's) between tubules (arrows) demonstrates early development of fibrotic regions. The asterisk in the lower right panel (periodic acid-Schiff) shows the region of cellular infiltration. Bars depict 100 μm. **b** In the upper part representative images used for total proportional area analysis. The results are summarized in the bar graphs. Low-Na represents the preparation through prefeeding of a low-sodium diet for more than 2 weeks. Each group includes 6 animals. * $p < 0.05$ meloxicam low-Na vs. either meloxicam normal diet or celecoxib low-Na diet; ** $p < 0.05$ celecoxib low-Na diet vs. meloxicam normal diet.

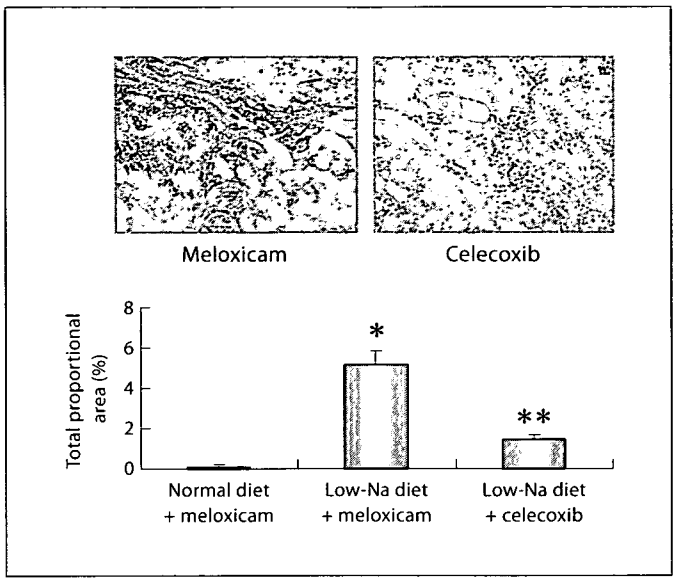

Fig. 5. Tubulointerstitial infiltrating F4/80-positive cells. Either meloxicam or celecoxib was administered for 4 weeks on a low-Na diet. * $p < 0.05$ meloxicam low-Na diet vs. either meloxicam normal diet or celecoxib low-Na diet; ** $p < 0.05$ celecoxib low-Na diet vs. meloxicam normal diet.

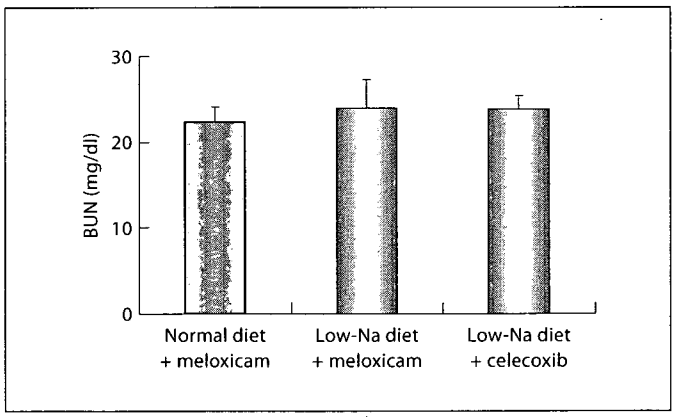

Fig. 6. Blood urea nitrogen (BUN) 4 weeks after starting either meloxicam or celecoxib. Each group includes 6 animals.

starting celecoxib, but others exhibited virtually no response (fig. 7a). Animals excreting higher amounts of urinary L-FABP than 50 μg/g creatinine during the follow-up period were defined as responders (n = 4). Those below that value were defined as nonresponders or low responders (n = 4). We evaluated the histological findings and quantified the degree of fibrosis 4 weeks later. As shown in figure 7b, the animals of the responder group showed a significant increase of their respective fibrotic regions compared to nonresponders ($p < 0.05$, n = 4 in each group). Correlations between urinary L-FABP and reciprocal of peritubular capillary blood flow 2 days after starting celecoxib are shown in figure 7c. Responders showed an increase of urinary L-FABP and reciprocal of peritubular capillary blood flow. In the responders, the more increased the reciprocal of peritubular capillary blood flow was, the more increased the urinary L-FABP level was. In nonresponders, both indicators showed no increase.

Discussion

The prescription of COX-2 inhibitors must be considered carefully, especially in geriatric individuals, though the selectivity of COX-2 theoretically better preserves renal function than regular NSAIDs. Chan et al. [16] investigated rheumatoid arthritis patients who had been prescribed either celecoxib or diclofenac and omeprazole for 6 months and found hypertension, peripheral edema, and renal failure in 24% of the celecoxib group and in 31% of the diclofenac and omeprazole group. Furthermore, renal failure was observed in 5.6% of the 144 celecoxib-treated patients and in 6.3% of those treated with diclofenac and omeprazole. The markets for these geriatric medications are saturated in the United States, but are increasing in Europe and in eastern Asian countries such as China, Korea, and Japan. Therefore, the chance of their prescription for pain relief is still increasing internationally. The renin-angiotensin-aldosterone system of such individuals is often at a higher level than that of younger individuals. This study was intended to examine the efficacy of urinary L-FABP to detect the risk of renal injury and to reveal chronic renal injury after intake of either meloxicam or celecoxib on a low-sodium diet, which easily upregulates the renin-angiotensin-aldosterone system. As expected, the peritubular capillary blood flow was significantly decreased in animals of the meloxicam and low-salt group 48 h after starting administration. The urinary L-FABP concentration of these animals had already increased at 24 h (fig. 1); the lower blood flow was established during the first 24 h. However, the other urine indicator, NAG, was insensitive to these hypoxic renal conditions (fig. 1, 2). We recently investigated living-related kidney transplantation and found a direct correlation between renal peritubular capillary flow and level of urinary L-FABP [15]. The evidence described here again confirmed urinary L-FABP as a biomarker of tubular hypoxic conditions. Moreover, animals that were adminis-

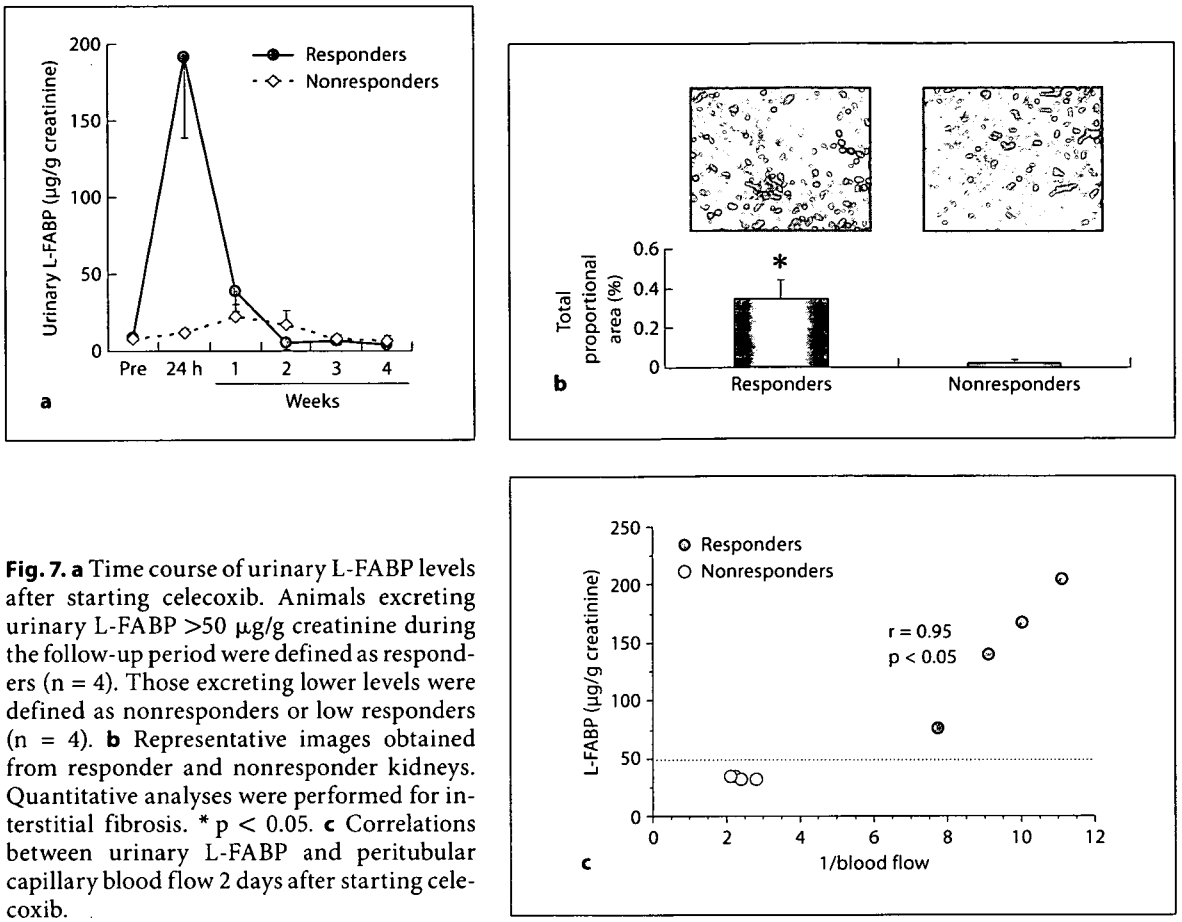

Fig. 7. a Time course of urinary L-FABP levels after starting celecoxib. Animals excreting urinary L-FABP >50 μg/g creatinine during the follow-up period were defined as responders (n = 4). Those excreting lower levels were defined as nonresponders or low responders (n = 4). **b** Representative images obtained from responder and nonresponder kidneys. Quantitative analyses were performed for interstitial fibrosis. * $p < 0.05$. **c** Correlations between urinary L-FABP and peritubular capillary blood flow 2 days after starting celecoxib.

tered meloxicam on a low-sodium diet for 4 weeks exhibited a fibrotic region at the tubular interstitium. That level was significantly increased compared to the normal-diet group (fig. 4). The cellular infiltration was apparent occasionally in animals treated with meloxicam on a low-sodium diet; the dominant population of these infiltrated cells consisted of macrophages (fig. 5). The meloxicam dosage in this experiment was in the nontoxic range, and the serum L-FABP level 48 h after starting daily meloxicam administration was not significantly increased. The effect of blood L-FABP derived from liver and/or intestine on urine is negligible, and the dynamics of urinary L-FABP is essential. Therefore, the initial urinary L-FABP level after starting meloxicam will be a promising biomarker to detect renal interstitial damage. Actually, L-FABP transgenic mice express human L-FABP, and the L-FABP ELISA system exclusively detects human L-FABP. Therefore, the above observations will be applicable directly to the prophylactic monitoring of prescriptions of this type of medication in humans.

Similarly, celecoxib, administered to the low-salt diet group, partially reduced peritubular capillary blood flow 48 h after starting daily administration. The renal interstitial fibrosis observed after 4 weeks was not comparable to that induced by meloxicam, but showed a significant increase compared to meloxicam administered together with a normal diet (fig. 4). Macrophage infiltration was not significantly increased, but F4/80-positive cells were visible between tubules. The dose of celecoxib used in this study is not in the toxic range and has often been used in previous studies [9]. The peritubular capillary blood flow was decreased in some animals that were administered celecoxib on a low-sodium diet. Therefore, we investigated whether that difference might be monitored by the level of urinary L-FABP. Celecoxib was administered daily on a low-sodium diet and urine was collected. As displayed in figure 7a, some animals excreted L-FABP into urine transiently within 2 weeks after starting daily celecoxib administration (responders), but others did not (nonresponders). Kidneys harvested at 4 weeks showed quantitatively remarkable differences of peritubular fi-

brosis between urinary L-FABP responders and nonresponders (fig. 7b). At 2 days after starting celecoxib, the decrease of peritubular capillary blood flow correlated with the increase of urinary L-FABP (fig. 7c). The transient elevation of the urinary L-FABP level reflects the initial damage demonstrated by the decrease of peritubular capillary blood flow. This initial change of the hemodynamics in the kidneys is pivotal and might further affect the development of mild interstitial fibrotic regions. The transient hypoxia despite the continuous administration of celecoxib might be because of some adaptation to hypoxia and further investigation will be necessary. Humans present a mixed population of responders and nonresponders whenever they are prescribed a certain medicine. Therefore, the observations from celecoxib and urinary L-FABP monitoring in this study might closely apply to a practical medical situation and be useful to distinguish between responders and nonresponders. To our knowledge, this is the first report providing evidence of a biomarker-predictable chronic COX-inhibitor-induced renal interstitial injury. It is reasonable to examine the humanized renal response to newly discovered compounds for potential drugs before starting clinical phase I trials, which will enable cost savings in pharmaceutical development. Exploring effective biomarkers and a suitable animal model representative of a certain pathophysiological condition will ensure the rapid translation of basic scientific discovery into new and better medical treatments, which is requested by the Critical Path Initiative Fact Sheet by the FDA 2006. The study described in this article will be a representative model for that mission.

Acknowledgments

This study was supported in part by grants from the Takeda Science Research Foundation (Osaka, Japan, to E.N.); the Cell Science Research Foundation (Osaka, Japan, to E.N.); Health and Labour Science Research Grants for Research on Human Genomes, Tissue Engineering, and Food Biotechnology, Ministry of Health, Labour and Welfare, Japan (No. 057100000661 to E.N., T.Y., and T.S.); the BioBank Japan Project on the Implementation of Personalized Medicine, MEXT (Ministry of Education, Culture, Sports, Science and Technology), Japan (No. 3023168 to E.N.); by Special Coordination Funds for Promoting Science and Technologies, MEXT, Japan (No. 1200015 to E.N.); by KAKENHI, MEXT, Japan (No. 19590935 to E.N. and T.S.); by NIH/NIDDK RO1-DK075976 (to D.P.), and by a Veterans Affairs Merit Award, USA (to D.P.).

References

1 Kramer HJ, Stinnesbeck B, Klautke G, Kipnowski J, Klingmueller D, Glaenzer K, Duesing R: Interaction of renal prostaglandins with the renin-angiotensin and renal adrenergic nervous systems in healthy subjects during dietary changes in sodium intake. Clin Sci (Lond) 1985;68:387–393.
2 Muther RS, Potter DM, Bennett WM: Aspirin-induced depression of glomerular filtration rate in normal humans: role of sodium balance. Ann Intern Med 1981;94:317–321.
3 Cryer B, Feldman M: Cyclooxygenase-1 and cyclooxygenase-2 selectivity of widely used nonsteroidal anti-inflammatory drugs. Am J Med 1998;104:413–421.
4 Vane JR, Bakhle YS, Botting RM: Cyclooxygenases 1 and 2. Annu Rev Pharmacol Toxicol 1998;38:97–120.
5 Gilroy DW, Colville-Nash PR, Willis D, Chivers J, Paul-Clark MJ, Willoughby DA: Inducible cyclooxygenase may have anti-inflammatory properties. Nat Med 1999;5:698–701.
6 Gabriel SE, Jaakkimainen L, Bombardier C: Risk for serious gastrointestinal complications related to use of nonsteroidal anti-inflammatory drugs. A meta-analysis. Ann Intern Med 1991;115:787–796.
7 Cheng HF, Wang JL, Zhang MZ, Miyazaki Y, Ichikawa I, McKanna JA, Harris RC: Angiotensin II attenuates renal cortical cyclooxygenase-2 expression. J Clin Invest 1999;103:953–961.
8 Cheng HF, Harris RC: Cyclooxygenases, the kidney, and hypertension. Hypertension 2004;43:525–530.
9 Engelhardt G, Bogel R, Schnitzler C, Utzmann R: Meloxicam: influence on arachidonic acid metabolism. II. In vivo findings. Biochem Pharmacol 1996;51:29–38.
10 Yamamoto T, Tada T, Brodsky SV, Tanaka H, Noiri E, Kajiya F, Goligorsky MS: Intravital videomicroscopy of peritubular capillaries in renal ischemia. Am J Physiol Renal Physiol 2002;282:F1150–F1155.
11 Matsumoto M, Tanaka T, Yamamoto T, Noiri E, Miyata T, Inagi R, Fujita T, Nangaku M: Hypoperfusion of peritubular capillaries induces chronic hypoxia before progression of tubulointerstitial injury in a progressive model of rat glomerulonephritis. J Am Soc Nephrol 2004;15:1574–1581.
12 Ogasawara Y, Takehara K, Yamamoto T, Hashimoto R, Nakamoto H, Kajiya F: Quantitative blood velocity mapping in glomerular capillaries by in vivo observation with an intravital videomicroscope. Methods Inf Med 2000;39:175–178.
13 Kamijo A, Sugaya T, Hikawa A, Okada M, Okumura F, Yamanouchi M, Honda A, Okabe M, Fujino T, Hirata Y, Omata M, Kaneko R, Fujii H, Fukamizu A, Kimura K: Urinary excretion of fatty acid-binding protein reflects stress overload on the proximal tubules. Am J Pathol 2004;165:1243–1255.
14 Noiri E, Nagano N, Negishi K, Doi K, Miyata S, Abe M, Tanaka T, Okamoto K, Hanafusa N, Kondo Y, Ishizaka N, Fujita T: Efficacy of darbepoetin in doxorubicin-induced cardiorenal injury in rats. Nephron Exp Nephrol 2006;104:e6–e14.
15 Yamamoto T, Noiri E, Ono Y, Doi K, Negishi K, Kamijo A, Kimura K, Fujita T, Kinukawa T, Taniguchi H, Nakamura K, Goto M, Shinozaki N, Ohshima S, Sugaya T: Renal L-type fatty acid-binding protein in acute ischemic injury. J Am Soc Nephrol 2007;18:2894–2902.
16 Chan FK, Hung LC, Suen BY, Wu JC, Lee KC, Leung VK, Hui AJ, To KF, Leung WK, Wong VW, Chung SC, Sung JJ: Celecoxib versus diclofenac and omeprazole in reducing the risk of recurrent ulcer bleeding in patients with arthritis. N Engl J Med 2002;347:2104–2110.

Original Article

A Water-Soluble Fullerene Vesicle Alleviates Angiotensin II–Induced Oxidative Stress in Human Umbilical Venous Endothelial Cells

Rui MAEDA[1),2)], Eisei NOIRI[1),3),4)], Hiroyuki ISOBE[1),2)], Tatsuya HOMMA[2)], Tamami TANAKA[4)], Kousuke NEGISHI[4)], Kent DOI[4)], Toshiro FUJITA[3),4)], and Eiichi NAKAMURA[1),2),5)]

A water-soluble fullerene vesicle based on the Buckminsterfullerene molecule ($Ph_5C_{60}K$, denoted as PhK) was explored to determine its effects on anti-oxidation of human umbilical endothelial cells (HUVEC) exposed to exogenous and endogenous reactive oxygen species (ROS). Hydrogen peroxide 0.05–0.25 mmol/L remarkably reduced the cellular viability of HUVEC. This reduction in viability was markedly improved when PhK 0.01–1 μmol/L was added simultaneously to the culture medium. The reduction of viability in HUVEC induced by angiotensin II (AII) 10^{-9} to 10^{-7} mol/L was improved by pretreatment with PhK 0.1 or 10 μmol/L 12 h before AII stimulation. The ROS indicator CM-H_2DCFDA demonstrated the efficacy of PhK 1 or 10 μmol/L in decreasing AII-induced ROS production to the level induced by the AII receptor blocker RNH-6470 20 μmol/L. The AII-induced peroxynitrite formation, as gauged using hydroxyphenyl fluorescein as a probe, was alleviated significantly by either pretreatment with PhK 0.1 or 1 μmol/L. Electron microscopy revealed intracellular localization of PhK in HUVEC after 12 h incubation. The PhK decreased the AII-induced apoptosis and lipid peroxidation processes as revealed by hexanoyl-lysine adduct formation. These observations show that the PhK water-soluble fullerene vesicle is promising as a compound controlling not only exogenous ROS, but also endogenous AII-mediated pathophysiological conditions. (*Hypertens Res* 2008; 31: 141–151)

***Key Words*: reactive oxygen species, endothelial cells, nano-compound, apoptosis**

Introduction

It has recently been suggested that angiotensin II (AII) is not simply an autacoid with hemodynamic and renal actions, but rather a biologically active mediator that imparts direct effects on endothelial and vascular smooth muscle cells. Actually, AII plays a key role in the initiation and amplification of pathobiological events leading to vascular disease. In addition, AII is a major mediator of oxidative stress and

From the [1)]Center for NanoBio Integration, [2)]Department of Chemistry, [3)]Department of Hemodialysis and Apheresis, [4)]Department of Nephrology and Endocrinology, The University of Tokyo, Tokyo, Japan; and [5)]Japan Science and Technology Agency, ERATO, Nakamura Functional Carbon Cluster Project, Tokyo, Japan.

Part of this study was supported by the NanoBio Integration Program, Ministry of Education, Culture, Sports, Science and Technology (MEXT), Japan (R.M., E.N., H.I., E.N.), by Health and Labour Sciences Research Grants for Research on Human Genome, Tissue Engineering Food Biotechnology from the Ministry of Health, Labour and Welfare, Japan (057100000661 E.N.), by a Grant-in-Aid for Scientific Research from the MEXT, Japan (19590935 E.N.), by the BioBank Japan Project on the Implementation of Personalized Medicine, MEXT, Japan (3023168 E.N.), by Special Coordination Funds for Promoting Science and Technologies, MEXT, Japan (1200015 E.N.), and by ERATO, JST, Japan (Nakamura Functional Carbon Cluster Project; E.N.).

Address for Reprints: Eisei Noiri, M.D., Department of Nephrology 107 Laboratory, University Hospital, The University of Tokyo, 7-3-1 Hongo, Bunkyo-ku, Tokyo 113-8655, Japan. E-mail: noiri-tky@umin.ac.jp

Received April 19, 2007; Accepted in revised form August 5, 2007.